JOURNAL OF GEOPHYSICAL RESEARCH, VOL. 105, NO. B6, PAGES 13,875–13,903, JUNE 10, 2000

Crustal structure and seismicity distribution adjacent to the Pacific and North America plate boundary in southern California

Egill Hauksson

Seismological Laboratory, Division of Geological and Planetary Sciences, California Institute of Technology, Pasadena

Abstract. New three-dimensional (3-D) V_P and V_P/V_S models are determined for southern California using P and S-P travel times from local earthquakes and controlled sources. These models confirm existing tectonic interpretations and provide new insights into the configuration of geological structures at the Pacific-North America plate boundary. The models extend from the U.S.-Mexico border in the south to the southernmost Coast Ranges and Sierra Nevada in the north and have a 15-km horizontal grid spacing and an average vertical grid spacing of 4 km, down to 22 km depth. The heterogeneity of the crustal structure as imaged by V_P and V_P/V_S models is larger within the Pacific plate than the North American plate. Similarly, the relocated seismicity deepens and shows more complex 3-D distribution in areas of the Pacific plate exhibiting compressional tectonics. The models reflect mapped changes in the lithology across major geological terranes such as the Mojave Desert, the Peninsular Ranges, and the Transverse Ranges. The interface between the shallow Moho of the Continental Borderland and the deep Moho of onshore California forms a broad zone to the north beneath the western Transverse Ranges, Ventura basin, and the Los Angeles basin and a narrow zone to the south, along the Peninsular Ranges. The near-surface increase in velocity, from the surface to up to 8 km depth, is rapid and has a logarithmic shape for stable blocks and mountain ranges but is slow with a linear shape for sedimentary basins. At midcrustal depths a rapid increase in V_P is imaged beneath the sediments of the large sedimentary basins, while beneath the adjacent mountain ranges the increase is small or absent.

1. Introduction

The boundary between the Pacific and North America plates in southern California is a region where many different geological terranes interact, forming a 200 to 300 km wide zone of transpressive deformation [e.g., *Powell,* 1993; *Atwater and Stock,* 1998]. Some of the models that explain how this deformation has evolved with time are flake tectonics [*Yeats*, 1981], microplate capture [*Nicholson et al.*, 1994], and propagating rift-subduction zone interactions [*Hey*, 1998]. These models provide explanations for some of the major recent events in the evolution of the plate margin, including initiation of seafloor spreading in the Gulf of California, rifting of the borderland, rotation of the Transverse Ranges, and intersection of an offshore propagating rift.

These tectonic events imprint the three-dimensional (3-D) crustal structure of southern California, including such terranes as the Continental Borderland, Peninsular Ranges, Imperial Valley, Transverse Ranges, Mojave Desert, southern parts of the Coast Ranges, southern San Joaquin Valley, and southern Sierra Nevada (Figure 1). On the basis of the inherited tectonic history of these terranes one would expect them to have different velocity structures. For instance, *Luyendyk et al.* [1980] proposed a model for Neogene crustal rotations in southern California to explain the relative juxtaposition of the different terranes. The superblock model by *Magistrale et al.* [1992] demonstrated such V_P variations on a regional scale using preassigned terrane boundaries inferred from surface geology.

Paper number 2000JB900016.
0148-0227/00/2000JB900016 $09.00

We use the available abundant earthquake data to determine 3-D crustal velocity models (V_P and V_P/V_S), which allows us to constrain potentially large velocity variations over short spatial scale lengths in southern California. In particular, we quantify lateral variations in V_P and V_P/V_S structure to depths of 20 to 25 km. In this study we determine V_P and V_P/V_S models without preassigned terrane boundaries and then calculate velocities with depth for individual terranes using a modified version of the Magistrale terrane boundaries. These models provide new information about velocity structure, including the 3-D shape of the near-surface velocity gradient and the velocity of the upper crust. In addition, we are interested in identifying the presence or absence of rapid change in velocities at midcrustal depth, sometimes referred to as the Conrad discontinuity. In many cases the presence of high-velocity lower crust may be evidence for a mafic lower crust [*Holbrook et al.*, 1992].

An additional goal of this study is to use the V_P and V_P/V_S velocity models to image the spatial relationship between terrane boundaries such as the San Andreas and other major late Quaternary faults. Because many of these faults have significant cumulative offsets, of the order of tens to hundreds of kilometers [e.g., *Irwin*, 1990], changes in velocity structure are likely to exist adjacent to these major faults. To infer terrane boundaries and rock composition from the V_P and V_P/V_S models, we use recent laboratory measurements of V_P and V_P/V_S in samples of variable rock compositions from *McCaffree Pellerin and Christensen* [1998].

As one application of the new 3-D V_P and V_P/V_S models, we relocate the southern California seismicity from 1981 to 1998. We provide a refined hypocentral distribution to facilitate comparison of the seismicity with the mapped active tectonic structures as well as features in the new 3-D velocity models. The refined hypocenters are more clustered and more realistically

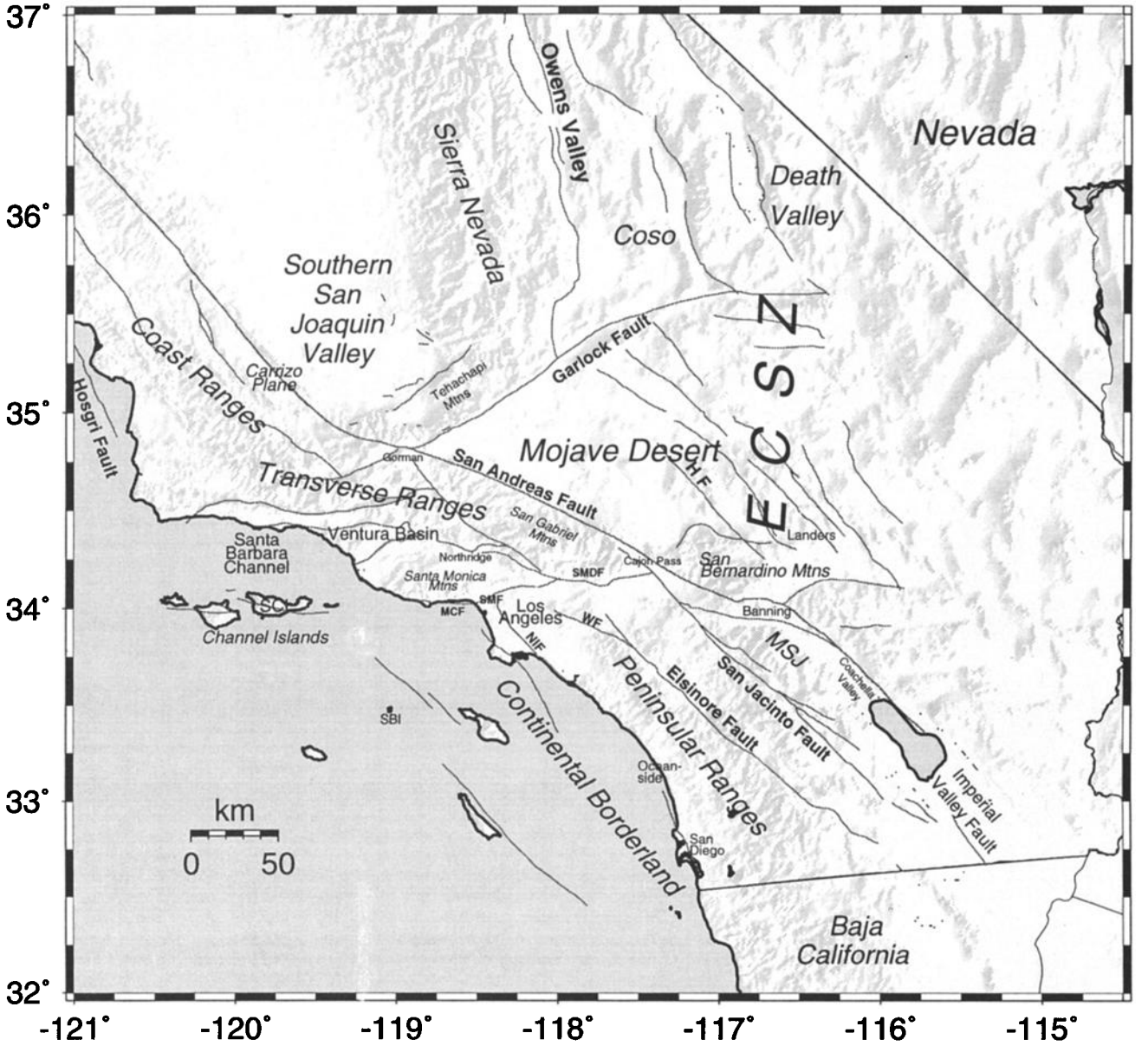

Figure 1. Map of study area showing the major geographical features in southern California. Major late Quaternary faults from *Jennings* [1975] are shown as solid lines. ECSZ, Eastern California Shear Zone; HF, Helendale fault; MCF, Malibu Coast fault; MSJ, Mt. San Jacinto; NIF, Newport-Inglewood fault; SBI, Santa Barbara Island; SJM, San Jacinto Mountain; SMDF, Sierra Madre fault; SMF, Santa Monica fault; WF, Whittier fault.

distributed with depth when compared to the hypocenters determined from the layered model of *Hadley and Kanamori* [1977]. Thus the new velocity models and the hypocenters provide a detailed image of ongoing tectonism.

By determining both V_P and V_P/V_S models for all of southern California we go beyond previous studies. On a regional scale the new V_P and V_P/V_S models agree with models from *Hauksson and Haase* [1997] that provide 10-km horizontal grid resolution for the greater Los Angeles basin. Most previous studies have used local earthquake data to determine only V_P models with lower spatial resolution or large-scale blocks [e.g., *Zhao and Kanamori*, 1992; *Magistrale et al.*, 1992; *Zhao et al.*, 1996]. Furthermore, the large data set used and the inversion for coarse and fine grid 3-D velocity models allow large velocity contrasts that in some cases are up to 60% between 15-km-spaced grid nodes, as compared to ±6% variations in many previous studies [e.g., *Zhao and Kanamori*, 1992].

2. Data and Approach

2.1. Data Set

Data from a subset of earthquakes recorded between 1981 and 1998 by the Southern California Seismic Network (SCSN), operated jointly by the U.S. Geological Survey (USGS) and California Institute of Technology (Caltech), were used in the inversion (Figure 2). The selected data set consists of 357,400 *P* arrival times and 52,600 *S-P* arrival times from 13,126 local

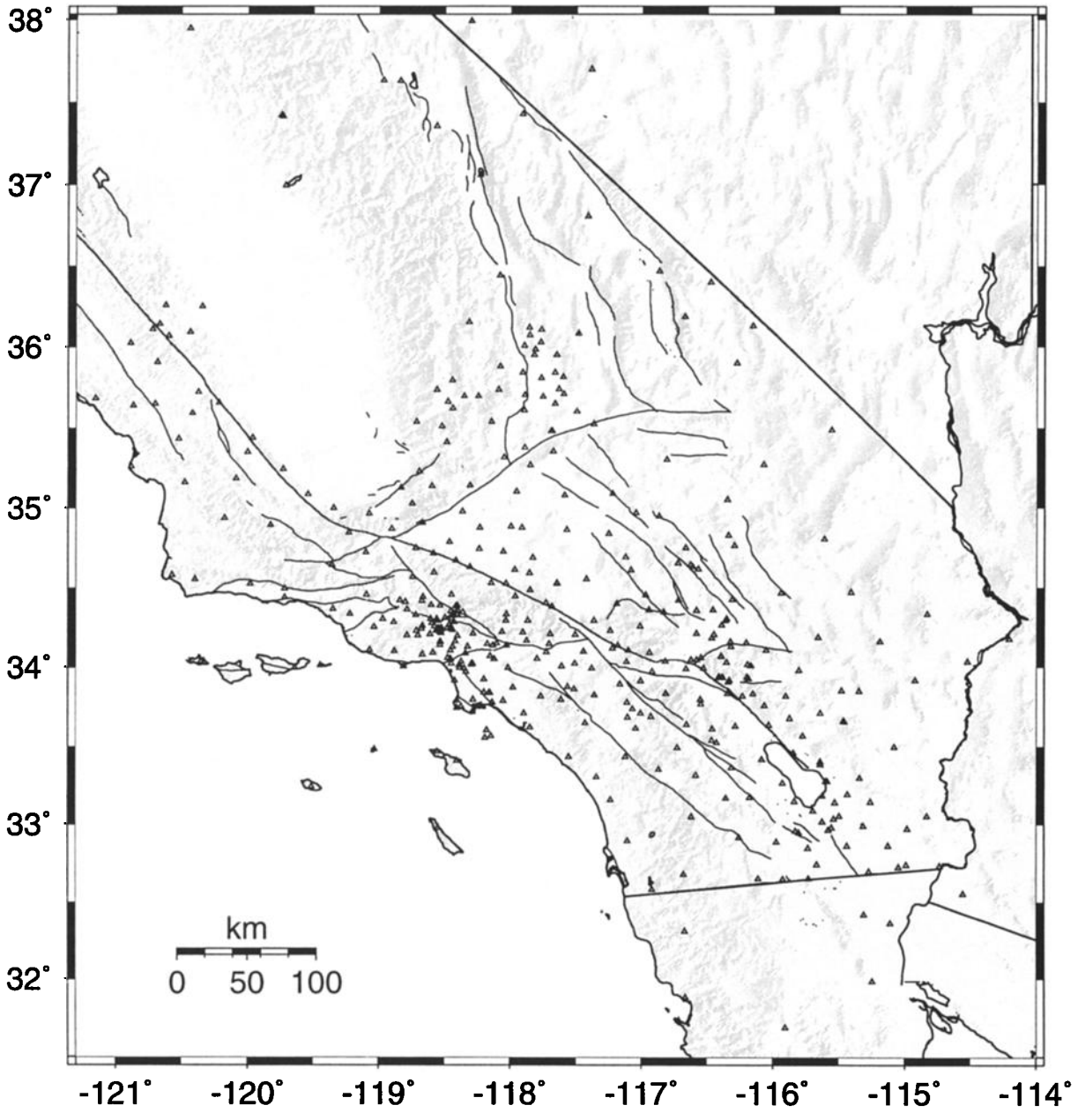

Figure 2. Seismographic stations of the Southern California Seismic Network (SCSN), operated jointly by the U. S. Geological Survey and the California Institute of Technology, recorded the P and S arrival times used in the inversions for V_P or V_P/V_S model.

earthquakes. These P and S wave arrival time picks (phase data) are available from the Southern California Earthquake Center, Data Center at Caltech. The S picks are incorporated in the inversion as S-P travel times to improve constraint on the focal depths and to determine a 3-D V_P/V_S model [*Thurber*, 1993].

The 13,126 earthquakes used in the inversion were selected from a data set of 305,000 events using the following criteria. First, all events of magnitude >3.1 with >20 picks, a total of 2829 events, were included. All these events are large enough to have clear arrivals at most of the stations in the network. Second, all events with magnitudes <3.1 with >20 picks and focal depths >15 km were included (5184 events). This group of deep events was selected for clarity of picks and for inclusions of direct ray paths. Third, to improve coverage in areas of low-seismicity events with magnitude <3.1, and depths <15 km, with >10 picks were added. These areas include the eastern California, western Mojave Desert, San Diego area, Continental Borderland, Coast Ranges, southern San Joaquin Valley, and northeastern Mojave extending into Death Valley and Nevada. In addition, ~1000 events from the Los Angeles basin for which picks are available from the University of Southern California, Los Angeles Basin Seismic Network were included. When available, picks recorded by portable experiments such as the 1992 Landers sequence [*Edelman and Vernon*, 1992] and the 1994 Northridge sequence [*Edelman et al.*, 1994] were included. For these data sets, however, careful analysis was required to avoid absolute timing

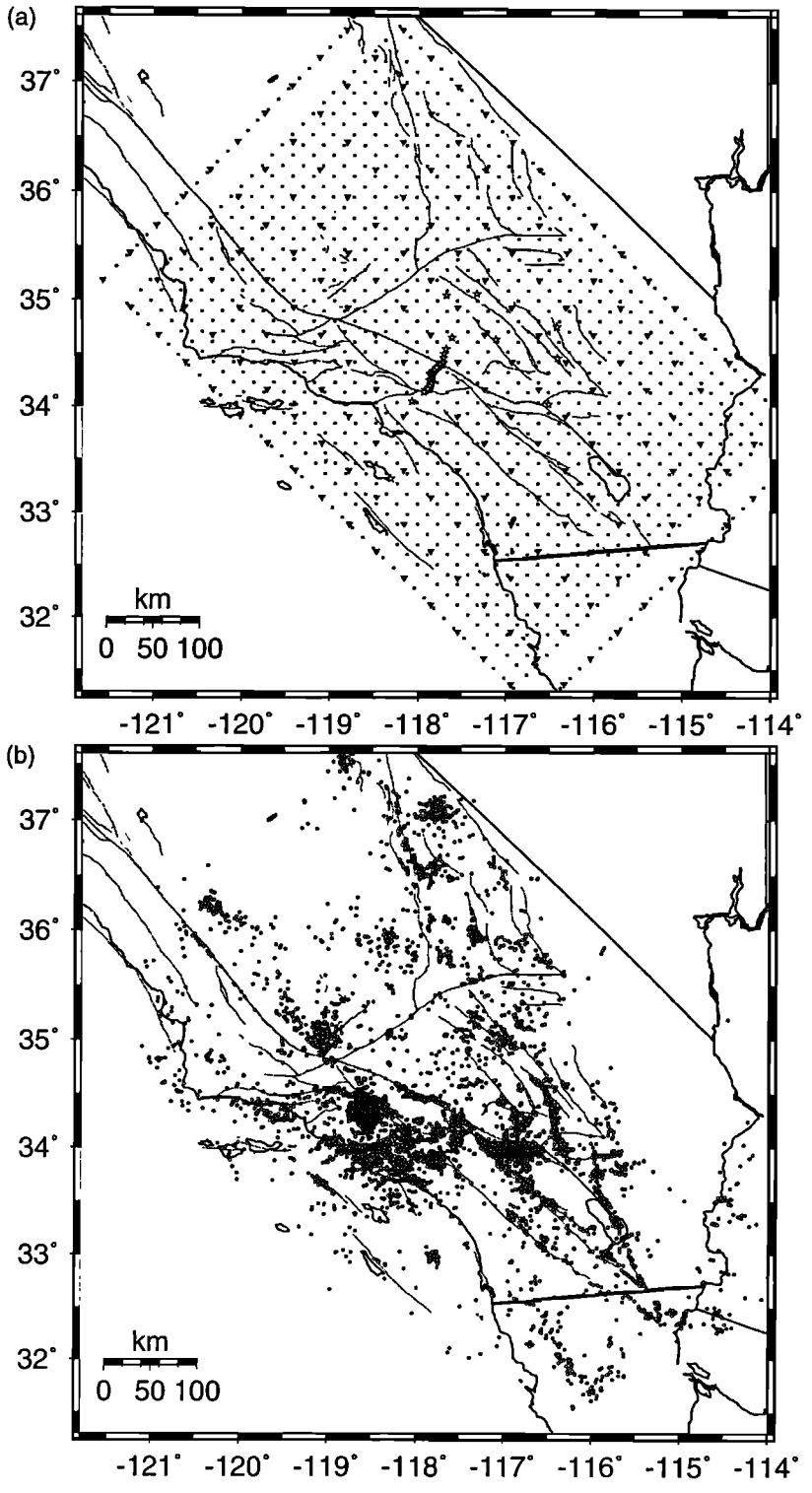

Figure 3. (a) The two 3-D velocity grids 40 km (inverted triangles) and 15 km (open squares) in horizontal dimension. Controlled sources (shots) are shown as stars. (b) The earthquakes (circles) (1981-1998) whose *P* and *S-P* arrival times were used in the inversion.

problems, which, in some cases led to rejection of the portable data.

Arrival times from 62 controlled sources (shots) recorded by the SCSN were also included to provide an absolute reference for the 3-D model and to constrain the shallow structure. We included the arrival times from the 49 shots that were part of the Los Angeles Region Seismic Experiment (LARSE) experiment [*Fuis et al.*, 1996], two (1981 and 1995) Catalina Island shots [*Given and Koesterer*, 1983; G. Fuis, written communication, 1995], two 1992 Landers shots [*Eberhart-Phillips and Mori*, 1994], several Mojave shots [*Kanamori and Fuis*, 1976], and a 1984 Azusa quarry shot (E. Hauksson, unpublished data, 1984).

2.2. Initial Velocity Model

The initial velocity model is a 3-D grid of points, with velocities linearly interpolated between the points. The model area coincides with the seismicity recorded by the SCSN and extends from northern Baja California, just south of the U.S.-Mexico border and the California-Arizona border in the south to Owens Valley and to the Carrizo Plane in the north (Figure 3). The depths of the horizontal grid layers are 1, 4, 6, 10, 15, 17, and 22 km. These depths were selected to model two major features, the near-surface gradient and the rapid increase in velocity at ~16 km which may be associated with lower crust of predominantly mafic composition.

The Moho boundary in the model is at 32 km depth beneath onshore California except beneath Imperial Valley, where the assigned Moho is at 22 km depth. The Moho depth for the Continental Borderland is also at 22 km. The grid nodes that define the shallow Moho at 22 km are allowed to vary in the inversion. To exclude most rays crossing the Moho boundary at 32 km depth, the ray lengths are tapered off at 120 to 140 km distance [*Magistrale et al.*, 1992]. This limits the model extent to depths between 22 and 25 km depending on local source-receiver geometry.

The commonly used velocity model for locating earthquakes in southern California is determined from the results of *Hadley and Kanamori* [1977]. We modified the velocity of their top layer to reflect the increase in V_P with confining pressure as shown by *Kanamori and Hadley* [1975]. The modified *Hadley and Kanamori* [1977] model that we use as our starting model is a good average model for the velocity structure of southern California. The final 3-D 15-km grid model (SC1-15) differs in average velocity from the starting model by <0.2 km/s for most of the layers (Figure 4).

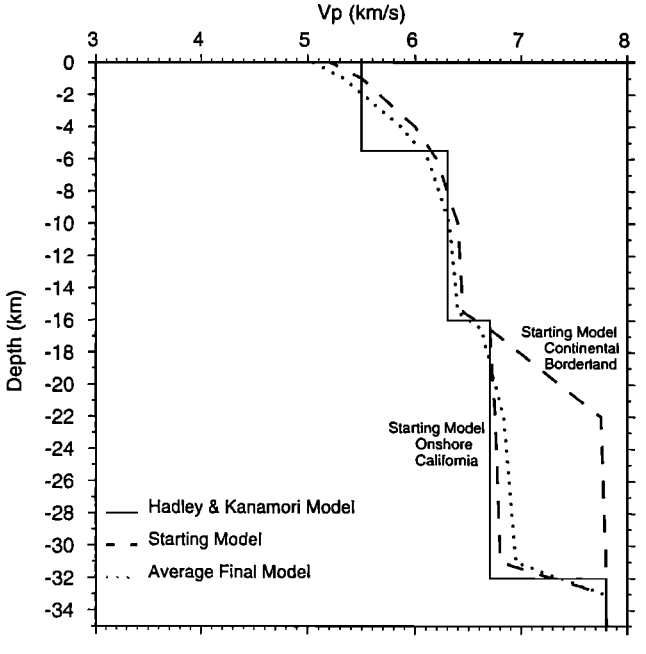

Figure 4. The V_P models as a function of depth, the *Hadley and Kanamori* [1977] model (solid), the interpolated starting model (SC0) (long dashes), and the final model (SC1-15) (short dashes, includes Continental Borderland in the average values). The starting model also includes the shallow Moho beneath the Continental Borderland, as the second set of dashed lines.

2.3. Inversion Approach and Parameters

We have applied the inversion method and computer algorithms (SIMULPS) developed by *Thurber* [1983, 1993] and *Eberhart-Phillips* [1990] (documentation provided by *Evans et al.* [1994]). Ray tracing is accomplished using an approximate 3-D algorithm with curved non planar ray paths [*Um and Thurber*, 1987]. The damped-least-squares solution to the linearized problem is obtained from

$$m = (M^T M + L)^{-1} M^T t,$$

where m is a vector of model perturbations, t is a vector of travel time residuals, L is a diagonal matrix of damping parameters, and M is a matrix of partial derivatives constructed according to the parameter separation techniques of *Pavlis and Booker* [1980]. Each of the two inversions we performed to create our final 3-D velocity model consisted of three model iterations, where each model iteration was followed by up to three iterations of hypocentral relocations using the latest velocity model.

We use the gradational inversion method, in this case using two inversions. This method consists of (1) starting with a horizontally uniform layered model (SC0) and inverting for a model (SC1-40) using a coarse 40-km grid; (2) interpolating the 40-km grid model with a 15-km grid; and (3) using the 15-km interpolated model as a starting model and relocated events to invert for a 15-km grid model (SC1-15). The outer edge of nodes was held fixed only in the 40-km grid inversion to prevent potentially large oscillations in velocity values near the edges of the model. The 15-km grid model was sufficiently stable and did not require fixing the outer nodes. We stopped at the 15-km grid because calculating a denser grid was too time consuming for the computer resources available. This gradational approach allows us to capture successively smaller wavelengths of the velocity structure into the model. It also allows for some inaccuracy in the starting model because we invert first for a coarse model using the 40-km grid which in essence provides a refined starting model. The data variances for the SC1-40 and SC1-15 models are listed in Table 1.

Because we expected extreme variations in velocity structure in the region, we used different inversion parameters than were used in other studies [e.g., *Eberhart-Phillips and Michael*, 1993]. Damping was used to stabilized the inversion. We kept the initial damping the same for the 40-km and 15-km grid models (150 for V_P and 15 for V_P/V_S). We did not invert for station delays as an additional model parameter to avoid trade-offs between the model parameters and because the station delays nearly all of the stations are located within the model region. The damping values of 150 and 15 were chosen by plotting data variance versus model length (defined here as the model standard deviation) and choosing a value that provided a reasonable trade-off between reduction in data variance and model length (see the appendix for further details about the damping). To further stabilize the inversion, we limited the maximum velocity perturbation to 0.5 km/s for each iteration in both the 40-km and 15-km grid models.

To test for some of the effects of parameterization, the horizontal grid layers were placed at different depths and the horizontal grid was rotated within the model area. All of these produced similar models to SC1-15, confirming that the final model SC1-15 is not dependent on the exact position of the initial grid. To evaluate the effects of uneven ray coverage, station

Table 1. Data Variance for the Three-Dimensional Velocity Models

Model	Grid, km	*P* Damping	*S-P* Damping	Number of of Iterations	Data Variance, s^2		Model Variance, km/s^2	
					Initial	Final	*P*	*S-P*
SC1-40	40	150	15	3	0.05689	0.04458	0.09599	0.00333
SC1-15	15	150	15	3	0.03028	0.02392	0.09876	0.00464

distribution, and data errors on the model, the full resolution matrix was determined. As discussed in the appendix, we use the diagonal elements of the resolution matrix (here referred to a resolution) calculated for the 15-km grid model to evaluate how well the final model parameters are resolved. The values of resolution range from 0 to 1.0, where 1.0 is perfectly resolved.

3. Geological Setting

These velocity models extend across the diverse geological terranes of southern California. Among these terranes are major batholiths such as the Peninsular Ranges where Cretaceous plutons intrude sedimentary and volcanic rocks of Jurassic age and metamorphic rocks of mostly unknown age [*Irwin*, 1990]. The models include the southern part of the Sierra Nevada batholith, made of mostly Cretaceous granitic rocks [*Irwin*, 1990]. The largest terrane within the model is the Mojave Desert, a predominantly Precambrian metamorphic and plutonic rocks that is partially covered by Paleozoic continental shelf deposits, intruded by Mesozoic plutons, and in limited places underthrust by schist [*Irwin*, 1990].

Other mountain ranges, such as the Transverse Ranges, Sierra Nevada, Tehachapi Mountains, and Coast Ranges, and a Mesozoic to Cenozoic accretionary prism [*Irwin*, 1990], are in these models. The late Cenozoic east-west trending Transverse Ranges can be divided into western Transverse Ranges, San Gabriels, and San Bernardino Mountains. The San Gabriels are an allochthon of Precambrian gneisses intruded by Mesozoic granitic plutons [*Ehlig*, 1981]. Within the San Gabriels the Vincent thrust separates upper plate crystalline rocks from the lower Pelona schist [*Ehlig*, 1981].

In addition, the models cover several active sedimentary basins such as the San Joaquin, Imperial, and Coachella Valleys and the Los Angeles and Ventura basins. The origins of the basins differ from a Jurassic to Cretaceous forearc basin with Quaternary alluvium in the San Joaquin Valley to the thick Upper Cretaceous and Tertiary deposits of the Santa Barbara, Ventura, and Los Angeles basins. The sediments of the Imperial and Coachella Valleys are Quaternary. The Imperial Valley covers an active spreading center [*Irwin*, 1990].

4. Results

4.1. V_P Model

The V_P 3-D model, consisting of seven layers ranging in depth from 1 to 22 km, is well resolved within most of the layers (Plate 1 and the appendix). The areas with sufficient ray density are shown in color in Plate 1. The well-resolved parts of the model are enclosed by the 0.3 resolution contour, which ranges from 0 to 1.0, with 1.0 being perfectly resolved. Along the edges of the model, in eastern California, offshore regions, and the San Joaquin Valley, the values of the resolution are small, <0.3, because few or no stations exist and the rate of seismicity is low. Within the 22-km-deep layer, near the bottom of the model, the area of significant resolution is confined to regions that have the deepest earthquakes. The average initial and final models are similar (Figure 4), in part because the starting model is well determined [*Hadley and Kanamori*, 1977] and the areas with large positive and negative velocity variations are of comparable spatial extent.

The three top layers of the V_P model at 1, 4, and 6 km depth have V_P changes of small spatial length (<50 km) reflecting the near-surface geology such as hard rock outcrops and late Quaternary sedimentary deposits. In particular, these layers include the surficial expression of the Los Angeles and Ventura basins, Imperial Valley, and southern San Joaquin (low velocities), and the major mountain ranges such as the Peninsular Ranges, the Transverse Ranges, the southern Sierra Nevada, and the Coast Ranges (higher velocities). For instance, the calculated velocity contrast within the 1-km-deep layer in the Los Angeles basin and the Santa Monica Mountains ranges from 3.57 to 6.02 km/s or 60%, reflecting basin sediments adjacent to hard rock outcrops. In contrast within the San Gabriel Mountains, the V_P within the 1-km-deep layer ranges from 5.53 to 6.19 km/s or 12%, showing smaller spatial variations within a coherent block. Between the 6 and 10 km deep layers all of the major basins, except the Ventura basin, have bottomed out (Plates 1c and 1d).

The V_P model provides some information about the internal properties of the different geological terranes. The 10-km-deep layer is the best resolved layer and may be the best representation of the shape of the terranes at depth (Plate 1d). The most significant features of this layer are the high-velocity ridges beneath the Santa Monica Mountains and the Channel Islands, San Joaquin Valley and the Tehachapi Mountains, the Peninsular Ranges, and a small feature beneath the Imperial Valley. These ridges may represent lower crustal rocks, which have been elevated into the upper crust. Another feature of this layer is the apparent similarity of the Mojave block velocities with the Coast Ranges block velocities. Reversing the right-lateral offset along the San Andreas fault by a minimum distance of 200 to 250 km would make these similar velocities form a continuous region.

The layers at 15 and 17 km depth contain velocities within the boundary zone between the lower and upper crust (Plates 1e and 1f). *Hadley and Kanamori* [1977] identified a 0.4 km/s velocity discontinuity at 16 km depth, which we call top of the lower crust. Assuming that the top of the lower crust is at ~16 km depth, the variations in V_P in the 15- and 17-km slices show the topography of the interface between lower and upper crust. These variations are most prominently displayed as high V_P that are present beneath the Santa Barbara Channel, western Peninsular Ranges, southern San Joaquin Valley, the Tehachapi Mountains, Santa Monica Mountains, and the Coachella and Imperial Valleys, locations which are similar to the 10-km depth.

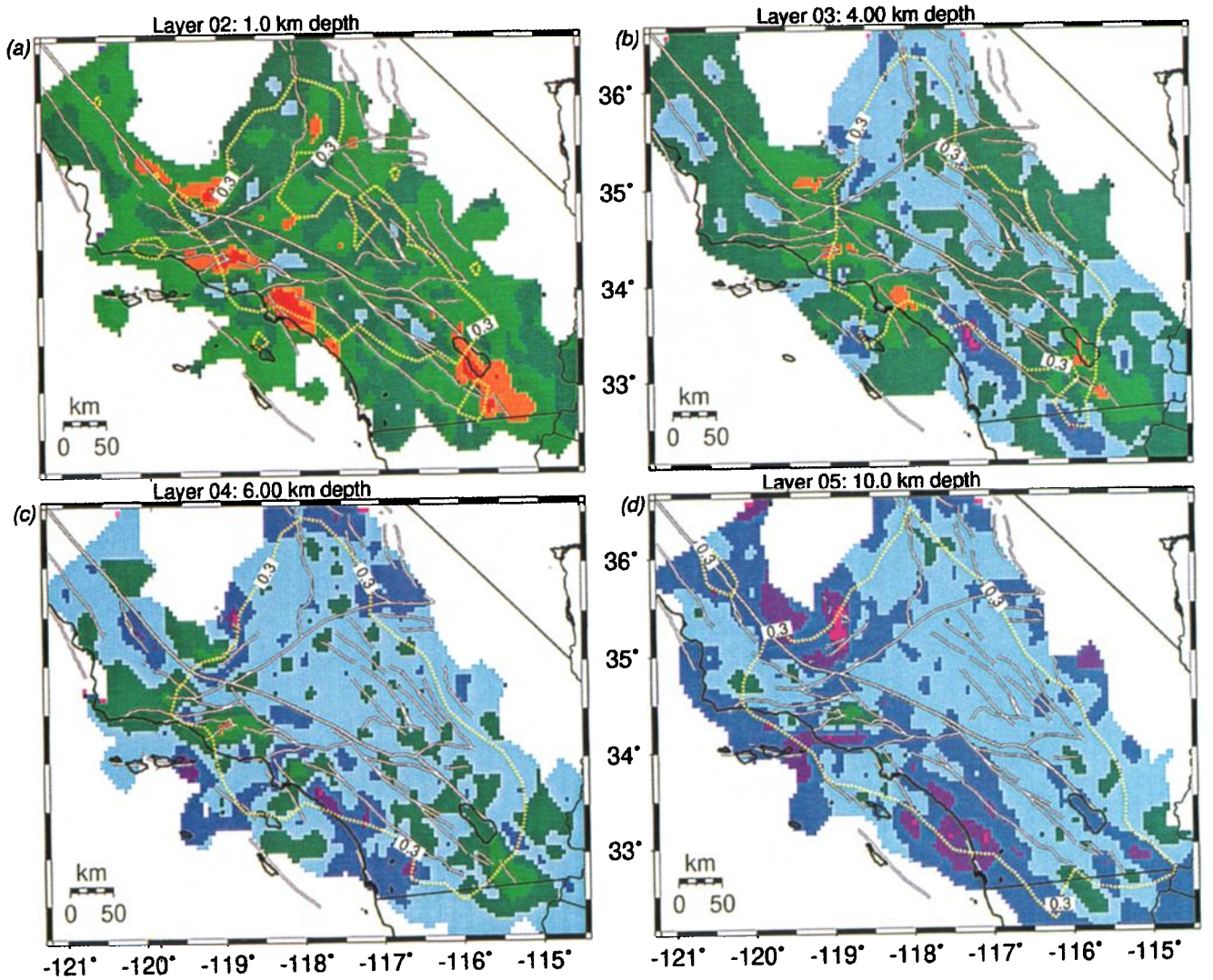

Plate 1. The final V_P 15-km grid model (SC1-15) shown in depth slices at (a)1,(b) 4, (c) 6, (d) 10, (e) 15, (f) 17, and (g) 22 km depth . Major late Quaternary faults are also shown as dashed lines. Model areas with adequate ray coverage have derivative weighted sum (DWS) values of 1000 or greater and are shown in color; see the appendix. The model is well resolved within the 0.3 values of the diagonal elements of the resolution matrix from the 15-km horizontal grid that are also shown (dashed contours). (h) Initial V_P model at 22 km depth, including the 15-km velocity grid points. See Figure 1 for geographical and fault names.

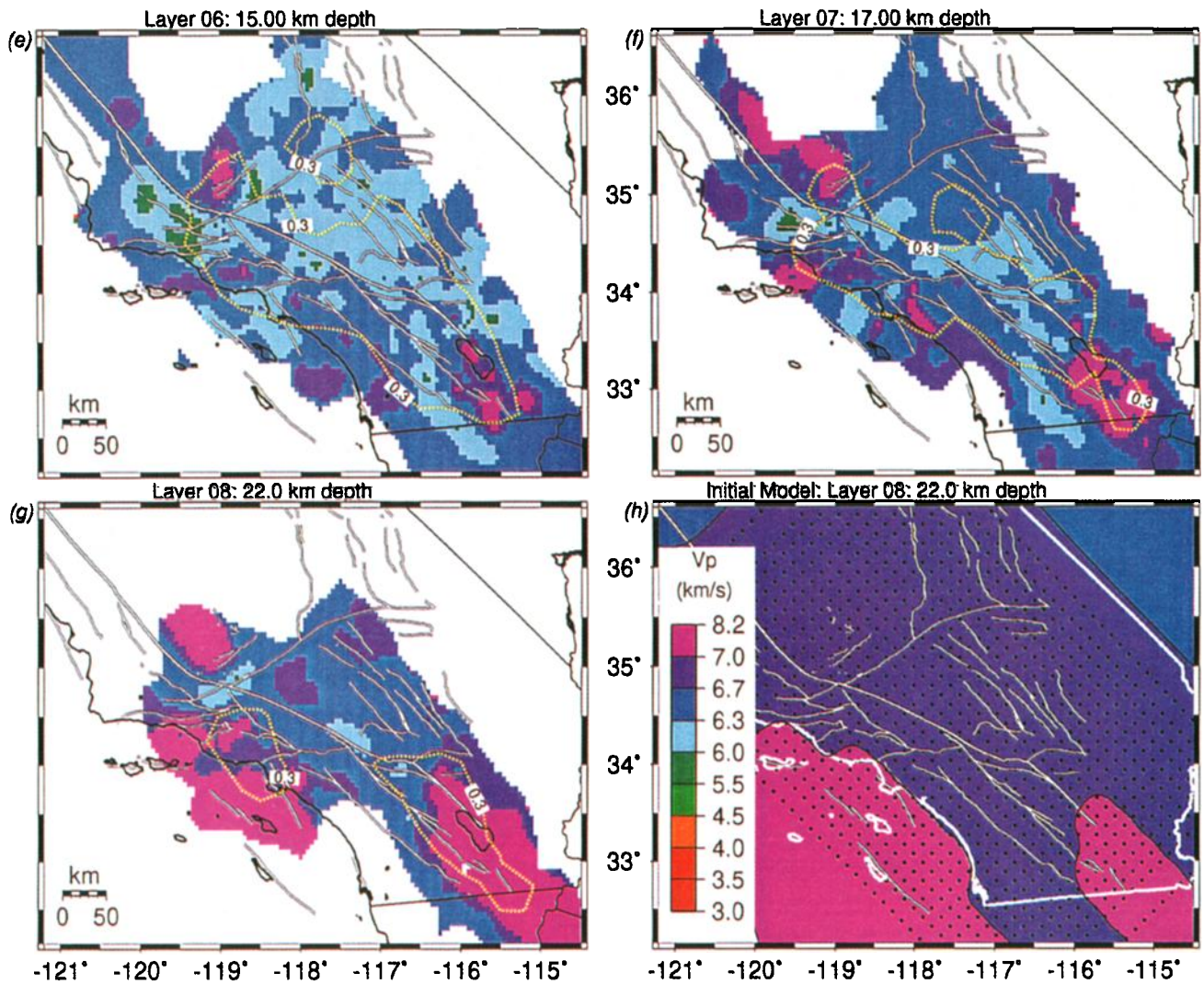

Plate 1. (continued)

The starting model included previously determined depths to Moho beneath the Continental Borderland [e.g., *Keller and Prothero*, 1987; *Fuis and Mooney*, 1990] and the Imperial Valley [*Parsons and McCarthy*, 1996]. We used the coastline as a boundary for the velocity step in our initial model. The inversion can change velocities across this boundary as needed to fit the data. The initial model within the 22-km-deep layer is modified significantly in the final 3-D model beneath the Imperial Valley by extending the zone of high V_P about 50 km farther to the northwest and adding some short-wavelength features to its shape (Plates 1g and 1h). Similarly, beneath the Santa Barbara Channel, Ventura basin, southern San Joaquin Valley, and southeastern part of the Los Angeles basin the high V_P lower crust extends up to anomalously shallow depths.

4.2. V_P/V_S Model

The areal extent of the V_P/V_S model is similar to that of the V_P model except for the 15-, 17-, and 22-km-deep layers where the resolved areas are significantly smaller (Plate 2). The areas with sufficient ray density are shown in color in Plate 2. The well-resolved parts of the model are enclosed by the 0.3 resolution contour. The *S-P* data are ~15% of the total data set, and the *S* arrival times in most cases are determined from vertical component seismograms. Because such *S* picks can be contaminated by converted phases, they are of lower quality than *S* picks from horizontal instruments. Further, when compared to the V_P model, the V_P/V_S model has overall lower resolution and should be viewed as a preliminary first-order model that will be improved as more *S* picks from three-component data become available. The V_P/V_S starting model was 1.73, which is the value commonly used for locating earthquakes in southern California. The V_P/V_S model shows both near-surface variations of short spatial length and regional long spatial length variations at depth, with overall variations in V_P/V_S ranging from 1.2 to 2.56.

The 1-, 4-, 6-, and 10-km-deep layers show numerous V_P/V_S anomalies of short spatial wavelength (Plates 2a-2d). The layers at 1- and 4-km depth have large areas of high V_P/V_S and low V_P that coincide with the near-surface water-saturated sediments of major basins (Los Angeles, Ventura, and other sedimentary basins). In contrast, the western Mojave and the northern Peninsular Ranges have areas of low V_P/V_S and high V_P. In the 6-km-deep layer the high V_P/V_S from the basins disappears, except beneath the Ventura basin, and low V_P/V_S anomalies become more prominent (Plate 2c). The best resolved layer at 10-km depth shows small variations in V_P/V_S with moderately higher values in the coastal regions and beneath the Imperial Valley (Plate 2d). This layer also has small anomalies, with a 20 to 40 km diameter, of moderately low V_P/V_S within the eastern Peninsular Ranges, the Mojave Desert, and the parts of the Sierra Nevada, possibly reflecting the presence of granitic outcrops [*Christensen*, 1996].

The resolved parts of the model decrease significantly in extent within the 15-, 17-, and 22-km-deep layers (Plates 2e to 2g). Nonetheless, within the 15-km-deep layer, zones of moderately high V_P/V_S exist beneath the eastern Santa Barbara channel, the Ventura Basin, and parts of the southern Imperial Valley area. Although the resolved area is small in the 17- and 22-km depth slices, they show similar patterns as the layers above (Plate 2g). One possible explanation of high V_P/V_S and high V_P at depth is the presence of mafic rocks such as gabbroic intrusions [*Christensen*, 1996] rather than being caused by presence of fluids.

If the high V_P/V_S at depth was caused by fluids in the crust at depths greater than a few kilometers, we would expect high V_P/V_S and low V_P to be more common adjacent to the major faults, such as the San Andreas and the San Jacinto faults. Such anomalies adjacent to faults are not resolved in this study. High V_P/V_S at depths of >10 km, however, is in most cases only observed in regions of high V_P, suggesting a rock composition relationship rather than presence of fluids.

4.3. Geological Terrane Models

We have imaged significant regional variations in V_P and V_P/V_S across the diverse geological terranes of southern California. To determine average velocity depth profiles for each region, we have used a modified version of the blocks defined by *Magistrale et al.* [1992], which includes the 23 major terranes in southern California based on surface geology (Figure 5). Because the block boundaries are assigned, it is possible that some parts of adjacent blocks are being included in a block. For instance, the high V_P/V_S determined for the west San Gabriel Mountains may be a result of including a small part of the east Ventura basin as part of this block. Similarly, the east Ventura basin may extend further beneath the Santa Monica Mountains than is apparent from surface geology. Because most terranes include several tens of grid points, we presume that these effects are minor and view these profiles as representative of the average properties of these terranes.

4.3.1. V_P Depth Profiles. We have determined average V_P depth profiles for each of the blocks shown in Figure 5. To analyze these profiles we have grouped together similarly shaped profiles (Figure 6). The shape of the upper part of the profile shows V_P as a function of confining pressure and depends to first order on whether the geologic structures are hard rock outcrops or sediments. The lower part of the profile shows the presence or absence of a velocity contrast between the upper and lower crust. None of the profiles have enough resolution at depths below 22 km to provide information about the lower crust just above the Moho. In most cases the one sigma standard deviation for these average values is 0.2 to 0.4 km/s for the 1- and 4-km-deep layers and 0.1 to 0.2 km/s for the deeper layers.

The first group, stable blocks, includes the largest areas of southern California: the Mojave Desert, the southern Sierra Nevada, the Coast Ranges west of the San Andreas fault, the east Peninsular Ranges, and the Little San Bernardino Mountains (Figure 6a). These profiles are typical hard rock profiles with rapid increase in velocity in the near surface. Most of the profiles except for the western Mojave and the Little San Bernardino Mountains have a high gradient zone, which suggest a sharp Conrad discontinuity at depths of 15 to 17 km.

The major mountain ranges, including the San Gabriels, the Tehachapis, the San Bernardinos, the west Peninsular Ranges, and the Santa Monicas, form the second group (Figure 6b). They show irregular V_P depth profiles, with the San Bernardinos having the lowest V_P and the Santa Monicas having the highest V_P. The Santa Monicas and the west San Gabriels show prominent linear gradients, as opposed to logarithmic gradients observed for rocks at shallow depths, suggesting the presence of sediments. None of these profiles have a distinct midcrustal discontinuity except for the Tehachapis, which have a high V_P zone above 10 km depth and are also floored by a low-velocity zone. Similarly, the west Peninsular Ranges are also floored by a low V_P zone imaged by the 22-km-deep layer.

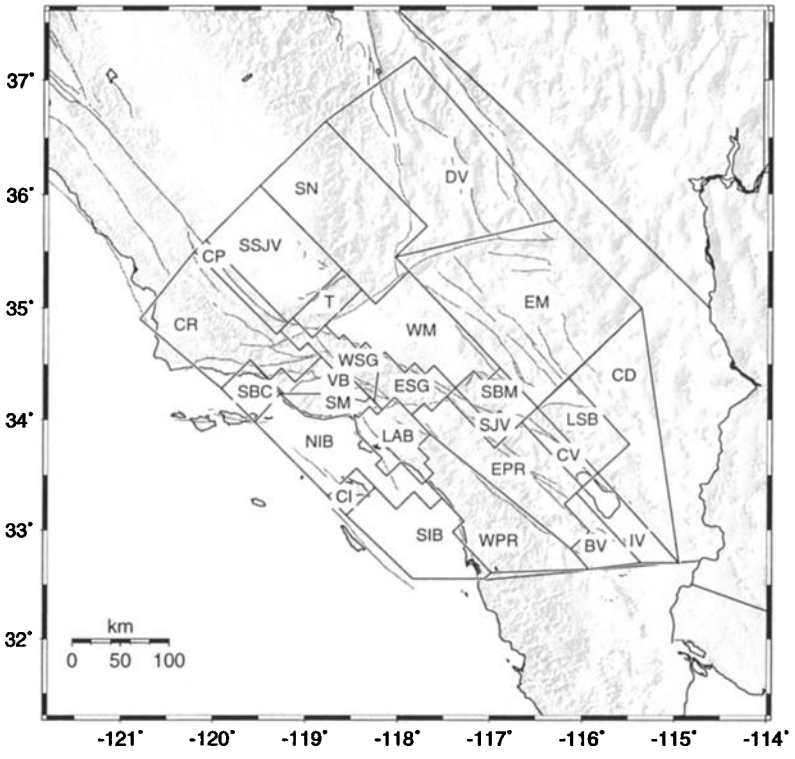

Figure 5. Map showing the assigned boundaries of tectonic blocks of southern California, modified from *Magistrale et al.* [1992] superimposed on a relief map. As part of the modification, the following terranes have been subdivided into two blocks, Peninsular Ranges, Mojave, and San Gabriels, and some of the block boundaries have been slightly modified to improve the match with surface geology. CR, Coast Ranges; CP, Carrizo Planes; SSJV, southern San Joaquin Valley; SN, Sierra Nevada; DV, Death Valley; SBC, Santa Barbara Channel; VB, Ventura basin; T, Tehachapi; WM, western Mojave; EM, eastern Mojave; WSG, west San Gabriel Mountains; ESG, East San Gabriel Mountains; SM, Santa Monica Mountains; SBM, San Bernardino Mountains; LSB, Little San Bernardino Mountains; CD, Colorado Desert; NIB, Northern Inner Continental Borderland; SIB, Southern Inner Continental Borderland; CI, Catalina Island; LAB, Los Angeles basin; EPR, east Peninsular Ranges; WPR, west Peninsular Ranges; SJV, San Jacinto Valley; CV, Coachella Valley; IV, Imperial Valley; BV, Borrego Valley.

Most of the basins that form the third group have slow linear increase in velocity in the near-surface that in extreme cases extend down to depths of 17 km (Figure 6c). The Ventura basin has the slowest V_P depth profile. Most of the basins show a prominent midcrustal velocity increase except for Imperial Valley, Borrego Valley, and Coachella Valley. The Coachella Valley is the only basin that has a slight low-velocity zone near 15 to 17 km depth. The amplitude of the Conrad beneath the basins is larger than found beneath the more stable areas in the first group, suggesting high V_P in the lower crust. The V_P profiles of the basin sediments compare well with the results of previous studies. For instance, in this study the smallest basin V_P in the Santa Barbara Channel is 3.4 to 4.1 km/s in the depth range down to 6 km depth, compared to the V_P of 2.5 to 4.0 km/s determined by *Keller and Prothero* [1987]. Because they have better resolution in the near surface and thus can more easily resolve the low near-surface velocities, we point out the agreement between the models at a depth of several kilometers.

The fourth group includes profiles from the Continental Borderland region (Figure 6d). Most of these depth profiles show linear gradients in the near surface. The steep gradient that starts at 15 km depth implies that the Conrad discontinuity is at 15 to 17 km depth, suggesting a thin lower crust on top of the shallow Moho at a depth of 22 to 25 km.

4.3.2. V_P/V_S Depth Profiles. The V_P/V_S depth profiles for the 23 major blocks have more variability than the V_P depth profiles but do show some general patterns (Figure 7). The average standard errors in the determination of the V_P/V_S ratios for each terrane range from 0.05 to 0.1. The stable block areas such as the Mojave Desert, southern Sierra Nevada, Coast Ranges west of the San Andreas fault, and the east Peninsular Ranges have average V_P/V_S values ranging from 1.67 to 1.95. The smallest V_P/V_S values are observed in the east Peninsular Ranges and largest values in the Coast Ranges west of the San Andreas fault. The V_P/V_S profiles for the topographically high regions show a large range of V_P/V_S 1.62 to 1.9. The Santa Monica Mountains block has the highest V_P/V_S, ranging from 1.90 in the near surface to 1.85 at depth. The Santa Monica Mountains and San Joaquin Valley regions have similar V_P profiles, but different V_P/V_S profiles, thus suggesting different lithology.

The basin areas of southern California have on the average higher values and a larger fluctuations in V_P/V_S, 1.69 to 2.2 at depths <10 km, decreasing to a range of 1.7 to 1.93 at depths greater than 10 km. In the near surface of the basins the high

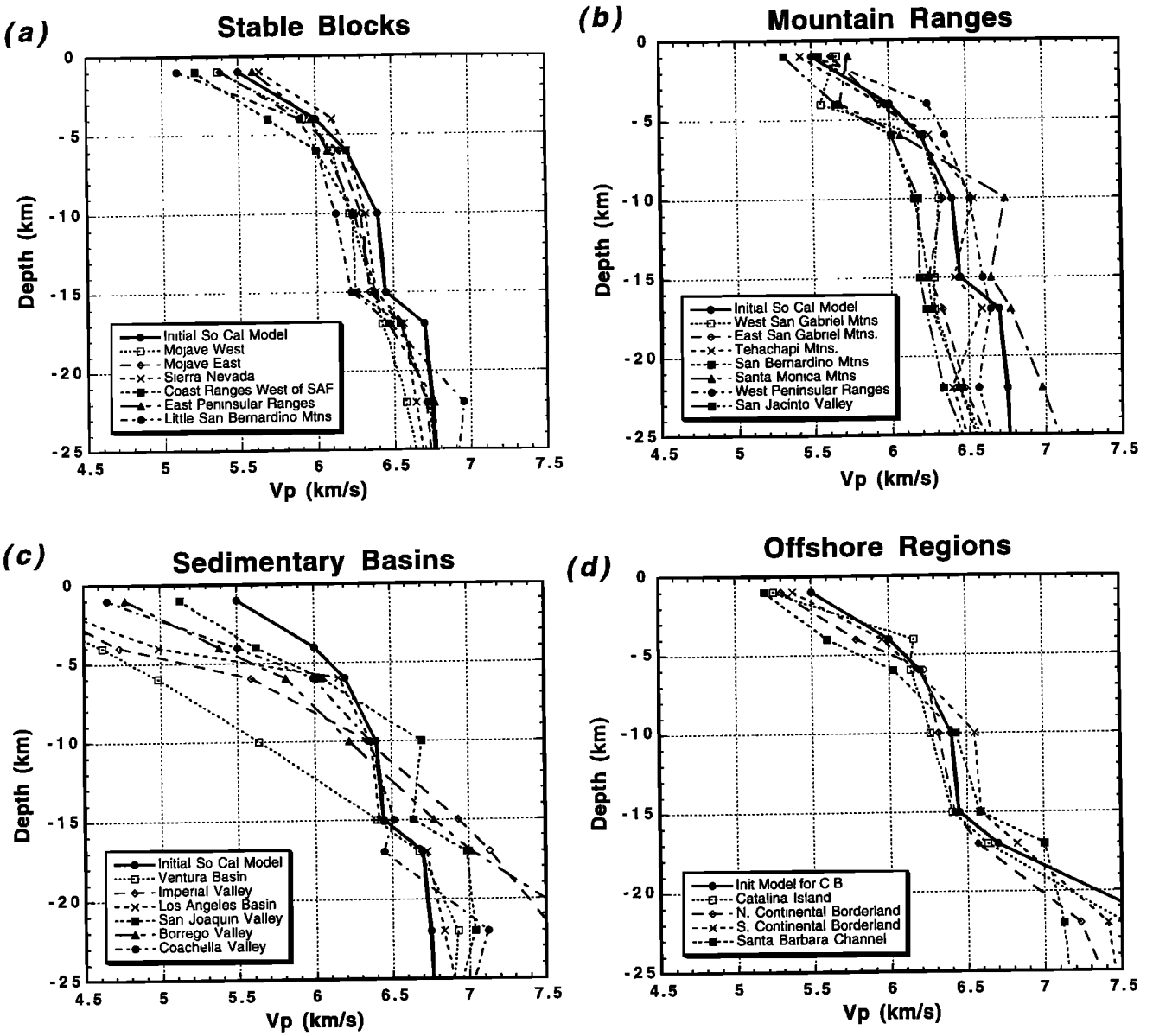

Figure 6. Profiles of V_P versus depth for the terranes defined in Figure 6. The initial model is shown as a solid line with solid circles; profiles for each terrane are shown with a different dash and symbol as shown in the legend. The deepest layer in the model is at 31 km depth. (a) Major stable terranes; (b) high elevation mountain ranges; (c) major basins and other regions with gradual increase in V_P down to depths of 8 to 15 km; and (d) offshore Continental Borderland (CB).

V_P/V_S may be related to high fluid content of near-surface cracks. At depth below the basins the V_P/V_S varies in the range from 1.75 to 1.8. These high values at depth suggest a more mafic crust beneath the basins than beneath the stable blocks.

The crust of the Continental Borderland has its own V_P/V_S signature, with values larger than the starting model (1.73), existing down to depths of 25 km. All the regions show high V_P/V_S at depths <10 km, while the Santa Barbara Channel has large V_P/V_S values from the surface down to 22 km depth.

4.4. Comparison With Existing Models

Magistrale et al. [1992] inverted for a superblock model of the southern California crust using fixed layer and block boundaries. We compare three of their profiles, Los Angeles basin, Tehachapi Mountains, and western Peninsular Ranges, with the profiles from the V_P model determined in this study (Figure 8). In general, the models are similar in the depth range of 5 to 14 km. At shallow depths (<4 km) the Magistrale model for the Los Angeles basin has lower V_P than the V_P model of this study. In contrast, for the Tehachapi Mountains and the west Peninsular Ranges, the Magistrale model has higher V_P at shallow depth. In the depth range of 14 to 25 km the Magistrale models for the three different blocks are similar to the initial model (Figure 8) while the models of this study show significant variations.

The overall differences between the models are not surprising. The differences at shallow depth suggest that it is difficult to constrain the shallow part of the crust using the earthquake data.

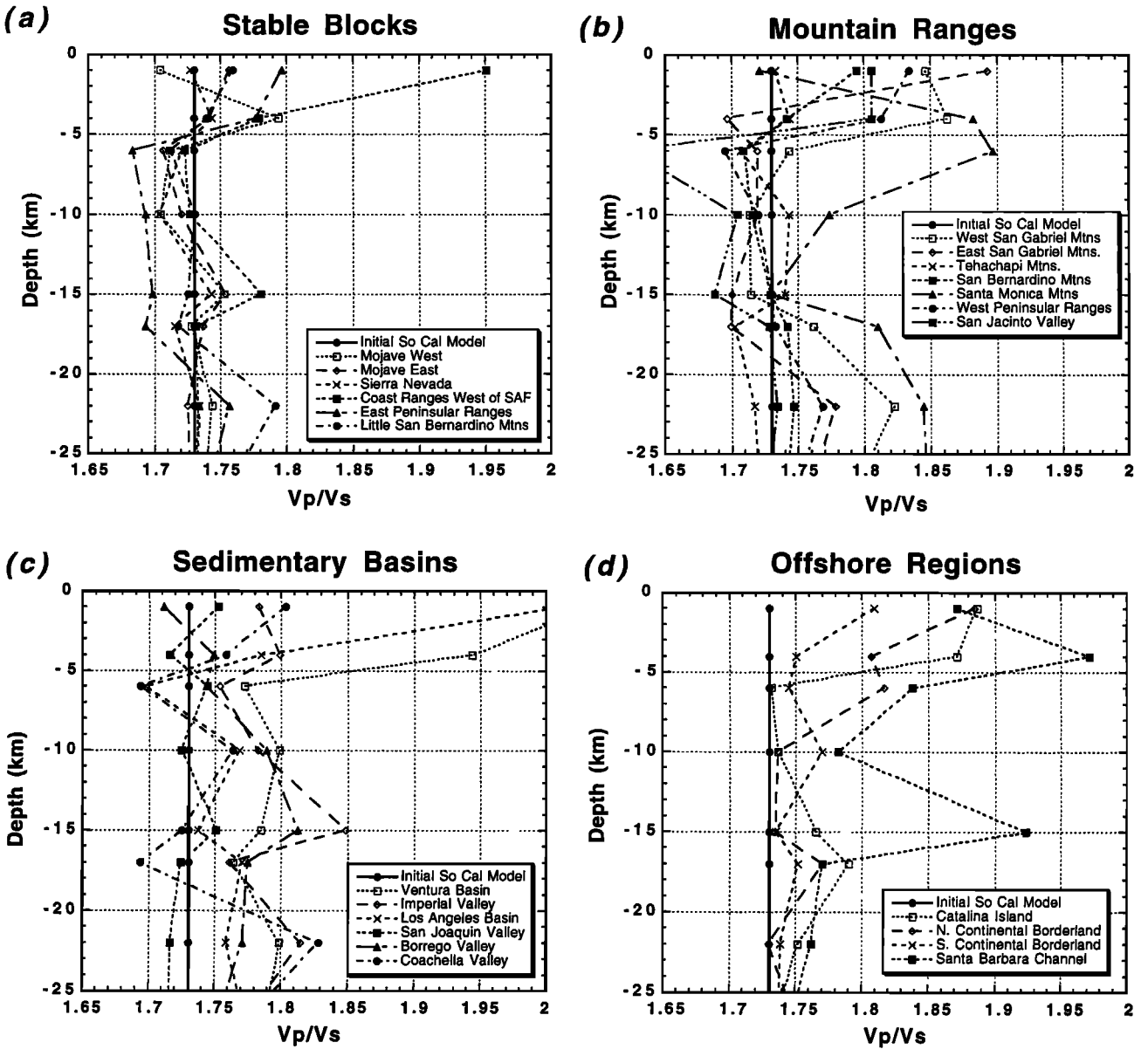

Figure 7. Profiles of V_P/V_S versus depth for the regions defined in Figure 5. See Figure 7 for detailed explanation.

At greater depths the fixed horizontal layer boundaries in the Magistrale model may make it difficult to resolve the correct velocity and layer thickness tradeoffs.

The V_P and V_P/V_S depth profiles of this study are similar to the models of *Hauksson and Haase* [1997] for the greater Los Angeles basin. Both models show similar regional patterns with high V_P beneath the basin sediments. The V_P/V_S depth profiles of this study are also similar to the results of *Nicholson and Simpson* [1985], who analyzed P and S-P travel time data from the San Bernardino Mountains and the north Peninsular Ranges, recorded by the SCSN. They found V_P/V_S ratios that ranged from 1.6 to 1.85 with values ranging from 1.75 to 1.85 in the near surface and 1.63 to 1.75 at depths >5 km.

4.5. Relocation of Shots

To test the applicability of using the 3-D velocity models to relocate hypocenters, we used the models to determine independently the hypocenters and origin times for 62 shots and compare these with true origin time and hypocenters (Figure 9). All of the shots have epicenters within 1 km of the true location except for two shots, whose epicenters are within 1.2 and 1.6 km distance, respectively.

The shot focal depths and origin times that were determined using the new models also show a general scatter within a limited range. The scatter in depth is small, with most of the hypocenters having depths within 2 km of the true depth. The tendency to increase the depth suggests that the near-surface V_P is slightly too high.

There are no obvious dependencies between changes in focal depth or origin time. The average 0.1 s bias in the origin times only explains about 0.3 to 0.5 km of the depth bias. The general scatter can be attributed to short-wavelength variations in the velocity structure that are not adequately modeled by a 15-km horizontal grid spacing. Overall, these results are a maximum estimate of our uncertainties associated with determining

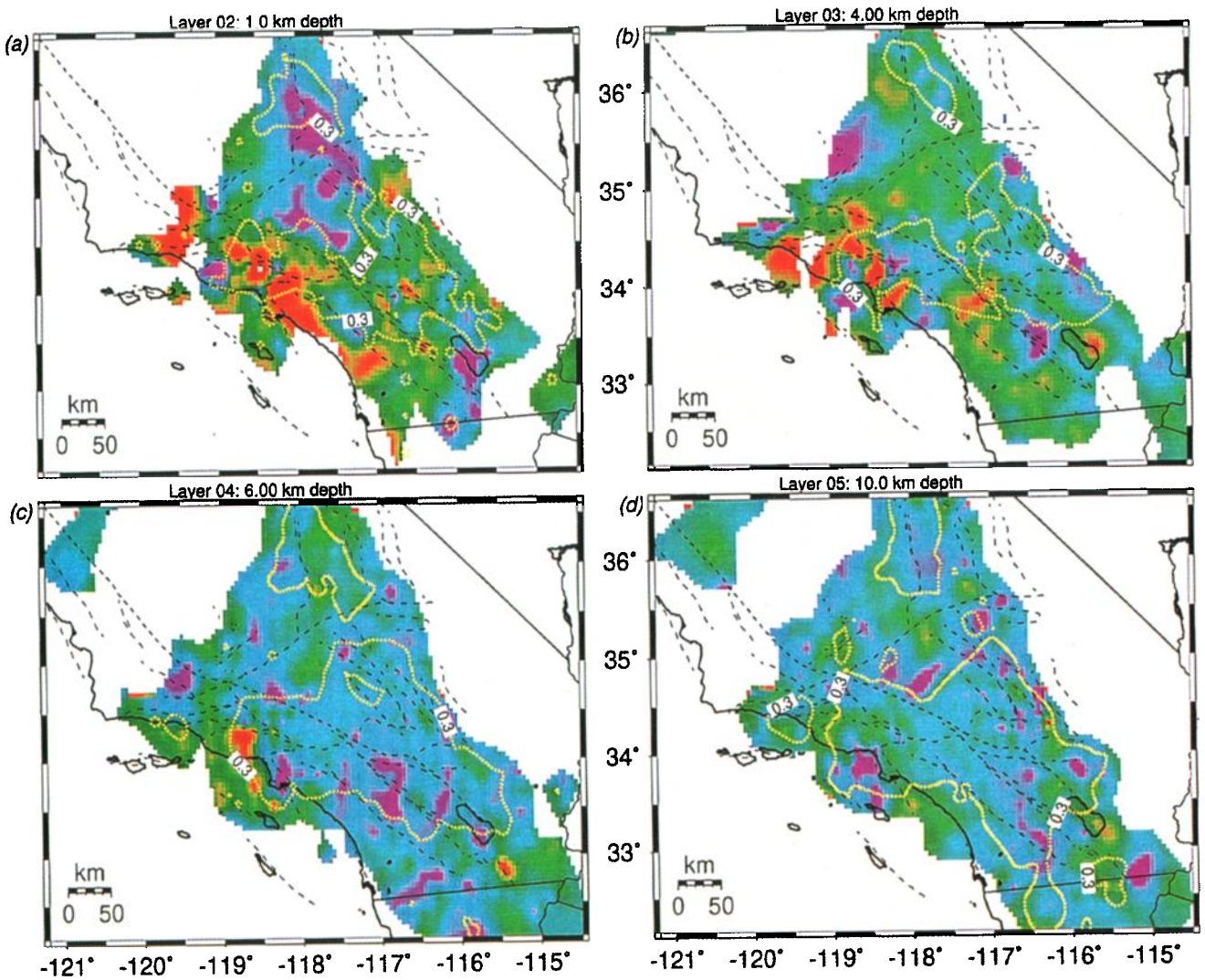

Plate 2. The final V_P/V_S 15 km grid model (SC1-15) shown in depth slices at (a)1,(b) 4, (c) 6, (d) 10, (e) 15, (f) 17, and (g) 22 km depth. Major faults are also shown as dashed lines. Model areas with adequate ray coverage have DWS values of 400 or greater and are shown in color; see the appendix. The model is well resolved within the 0.3 values of the diagonal elements of the resolution matrix from the 15-km horizontal grid are also shown (dashed contours). See Figure 1 for geographical and fault names.

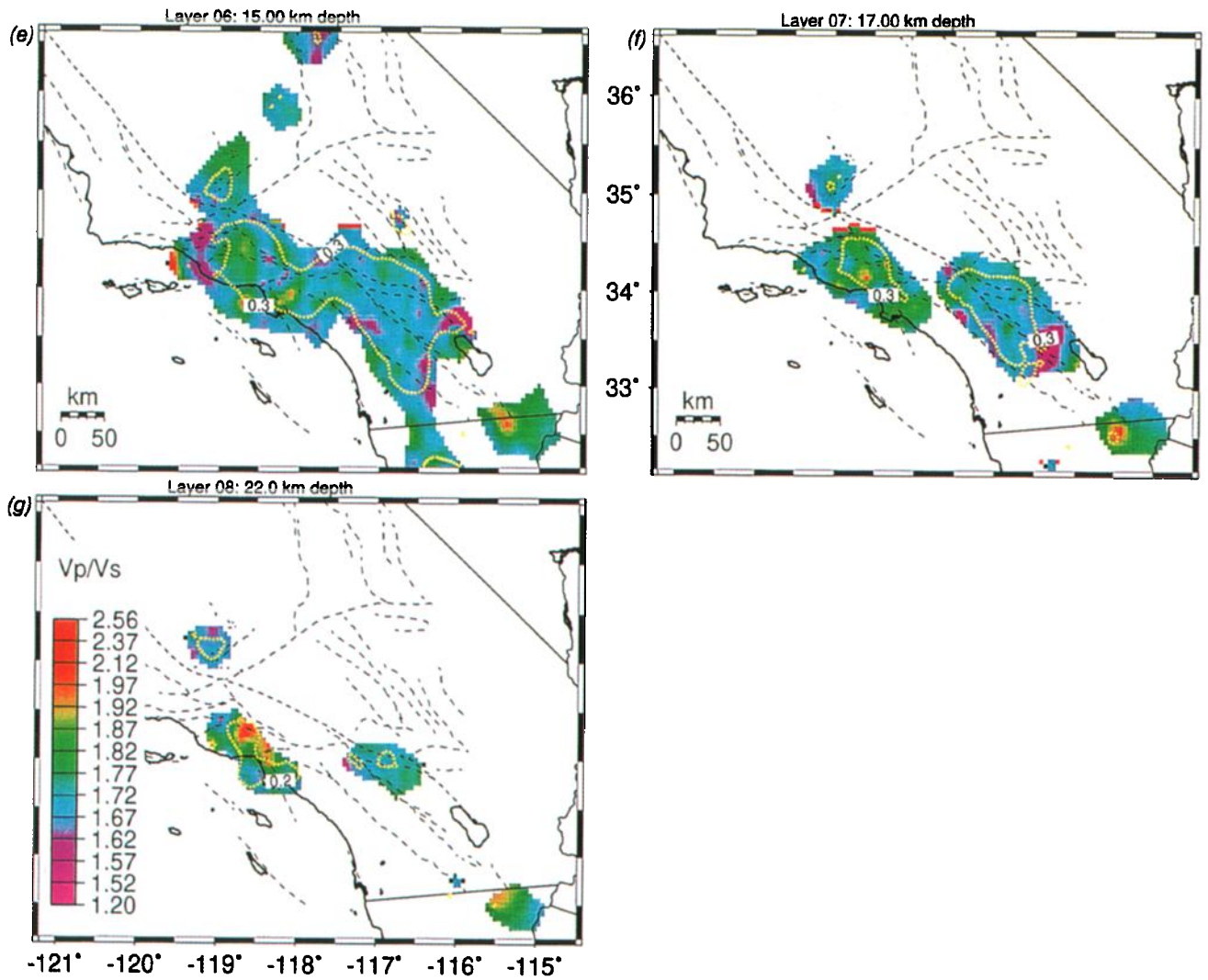

Plate 2. (continued)

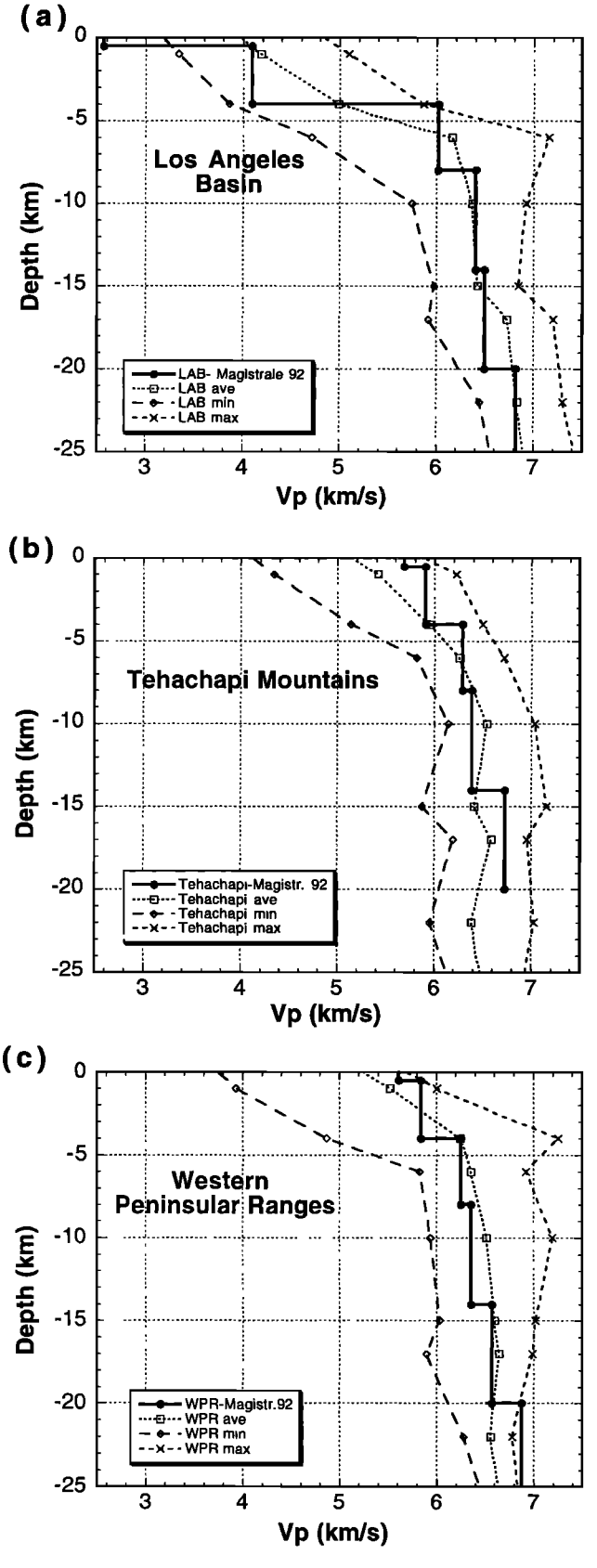

Figure 8. Comparison of three V_P depth profiles (shown as dashed lines with symbols as labeled in the legend) with the *Magistrale et al.* [1992] layered models (shown as solid lines connecting solid circles). Minimum and maximum V_P values for the respective profile from the 3-D model are also shown.

earthquake hypocenters using this 3-D model. In general, we would expect the scatter to be smaller for earthquakes because these are occurring at depth and their rays travel only once through the rapid velocity variations in the near surface.

4.6. Seismicity Distribution

The hypocenters of more than 305,000 earthquakes that occurred from 1981 to 1998 were redetermined using the new velocity models (Figure 10). Most of these events occurred in the depth range of 1 to 25 km where the 3-D velocity models are well constrained. For the data set of more than 13,000 events used in the 3-D model calculations the total root-mean-square residual (rms) was reduced from 0.28 s to 0.14 s. When the data set of 305,000 events was relocated, the overall distribution of residuals remains similar, but the average rms is reduced from 0.18 s to 0.09 s. The spatial distribution of the seismicity differs from previous distributions in that the various clusters are less scattered and in many cases form more coherent alignments along mapped late Quaternary faults. The hypocenters are improved because they include the 3-D velocity model that removes biases caused by 3-D effects in the structure. This new model, however, does not account for other effects such as larger SCSN station spacing at the edges of the network.

The relocations of the 305,000 events confirm many of the past observations about spatial distribution of seismicity in southern California. The numerous M>5 mainshocks and their aftershock sequences can be seen in Figure 10. The bulk of the background seismicity is located along the San Jacinto fault, Banning Pass segment of the San Andreas fault, the 1952 Tehachapi, the 1992 Landers aftershock zone, the 1994 Northridge, and near Coso. Significant activity occurs in Imperial Valley both north and south of the U.S.-Mexico border. Numerous northeast trends of seismicity can also been seen on both sides of the San Jacinto fault, suggesting conjugate faulting.

Most of the previously reported features of the southern California seismicity remain after recalculating the hypocenters using three-dimensional velocity models. For instance, the seismicity associated with the Mojave and Coachella Valley segments of the San Andreas fault does not coincide with the exact mapped surface trace similar to what *Jones* [1988] reported. Instead, the seismicity is offset from the fault trace, suggesting the background seismicity is not occurring on the rupture surfaces that accommodate major or great earthquakes. In contrast, the seismicity is densely clustered along the trace of the San Jacinto fault, suggesting a definitive spatial relationship between small earthquakes and rupture surfaces of large or major earthquakes. However, seismicity along the Elsinore fault is offset from the mapped trace like the San Andreas fault.

In the past the diffuse seismicity of southern California has been thought of as being an artifact because the strong velocity variations between the basin sediments and the rock outcrops in the nearby hills or mountains were not taken into account by the earthquake location algorithms. However, the Los Angeles area seismicity remains as diffuse as shown earlier by *Hauksson* [1990]; thus the refined hypocenters that were determined using the 3-D velocity models from this study confirm a complex 3-D distribution. The strongest seismicity trends center on the Newport-Inglewood and Whittier faults. The offshore seismic activity is less well constrained due to station coverage but nonetheless shows some significant clusters such as the 1986 Oceanside sequence and the Santa Barbara Island earthquake in 1981.

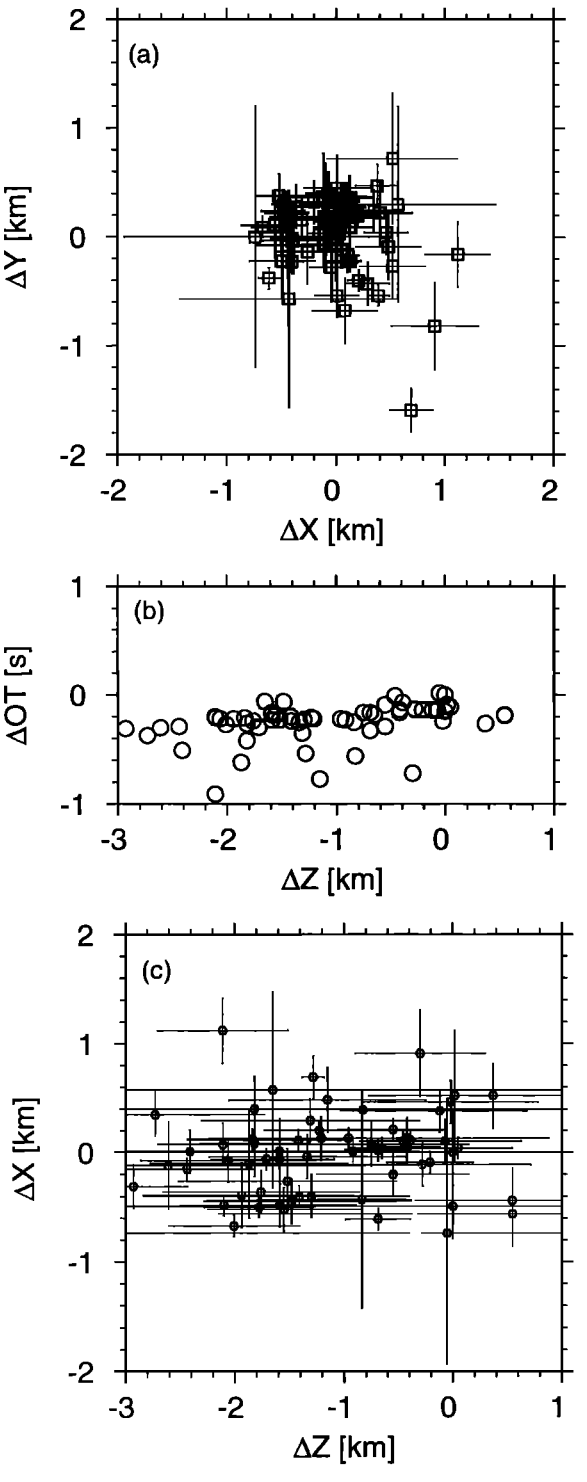

Figure 9. Summary of the 3-D relocations of the shots (timed explosions) using the SC1-15 model. (a) X and Y mislocations, where X is distance along N45°W. (b) Change in origin time versus change in depth. (c) Mislocation in X direction versus mislocation in depth.

5. Interpretation

The V_P and V_P/V_S models provide complementary information about rock composition. The two likely compositional end-members are mafic rocks with high V_P (>6.4) and high V_P/V_S (>1.8) and quartz rich rocks that have average V_P (~6.0 to 6.3) and low V_P/V_S (<1.7) [*Christensen*, 1996]. *McCaffree Pellerin and Christensen* [1998] collected rock samples in the San Gabriel Mountains and the Mojave Desert, adjacent to the LARSE I refraction line [*Fuis et al.*, 1996], and determined V_P and V_P/V_S as a function of confining pressure in the laboratory. In particular, they showed that Pelona schist has an average V_P of 5.8 km/s with 7% to 15% anisotropy and V_P/V_S of 1.67 with 6% to 20% anisotropy at 5 km depth. We use their measurements and rock composition interpretations to infer the average composition for some of the terranes. In particular, we discuss below how our V_P and V_P/V_S models contribute to the understanding of the distribution of Rand, Pelona, Orocopia, or other schist formations, inferred lithological variations within the Peninsular Ranges batholith, and the configuration of the eastern boundary of the Continental Borderland.

5.1. Distribution of Schist

Previous workers have inferred the presence of large contiguous areas of schist as part of the southern California crust. For instance, *Haxel and Dillon* [1978], and numerous other investigators have suggested that Pelona schist forms an accretionary wedge sequence that is in thrust contact with upper plate rocks of the entire western Mojave and the San Gabriel Mountains. In an independent study, *Burchfiel and Davis* [1981] described the occurrence of different types of schists in tectonic windows. Similarly, on the basis of depth of seismicity and an unpublished 3-D V_P model, *Magistrale and Zhou* [1996] inferred schist in the areas of the western Mojave Desert, Tehachapi Mountains, Coast Ranges west of the San Andreas fault, San Gabriel Mountains, and Banning Pass. They also proposed the presence of schist offshore, to the west of the Newport-Inglewood fault and south of the Malibu Coast fault. *Magistrale and Zhou* [1996] argued that areas underlain by schist formations have shallower (4-10 km) maximum depth of earthquakes than areas composed of other types of basement rock. Independently, *Malin et al.* [1995] suggested that the schist extended from the Tehachapi Mountains into the Mojave Desert. On the basis of seismic refraction data, *Fuis* [1998] and *Lutter et al.* [1999] also inferred schist beneath the San Gabriel Mountains along the LARSE I profile.

In contrast, *McCaffree Pellerin and Christensen* [1998] used their own data and the velocity profile from LARSE I, determined by *Lutter et al.* [1999], to analyze the bulk composition of the western Mojave. They argued that the Mojave gneiss forms the major lithology of the upper crust and that Pelona schist cannot be detected. Based on similar evidence a predominantly gneissic upper crust for the western Mojave was inferred from data from the Cajon drill hole by *Silver and James* [1988]. *McCaffree Pellerin and Christensen* [1998] also showed that a velocity decrease associated with the San Andreas fault is most likely associated with the Pelona schist that has been mapped at the surface only in the vicinity of the fault. They found that the San Gabriel terrane to the west of the San Andreas fault has V_P similar to San Gabriel gneiss and intrusives, with minor contributions of Mount Lowe intrusives and Pelona schist. They also interpreted a high-velocity anomaly near the San Gabriel fault as anorthosite and/or crustal granulitic gneisses.

In Figure 11a we compare our V_P depth profiles with *McCaffree Pellerin and Christensen's* [1998] for two different terranes. For comparison with the western Mojave block, we have chosen three rock velocity depth profiles, Mojave intrusives, Pelona schist, and Mojave gneiss. The V_P of the western Mojave

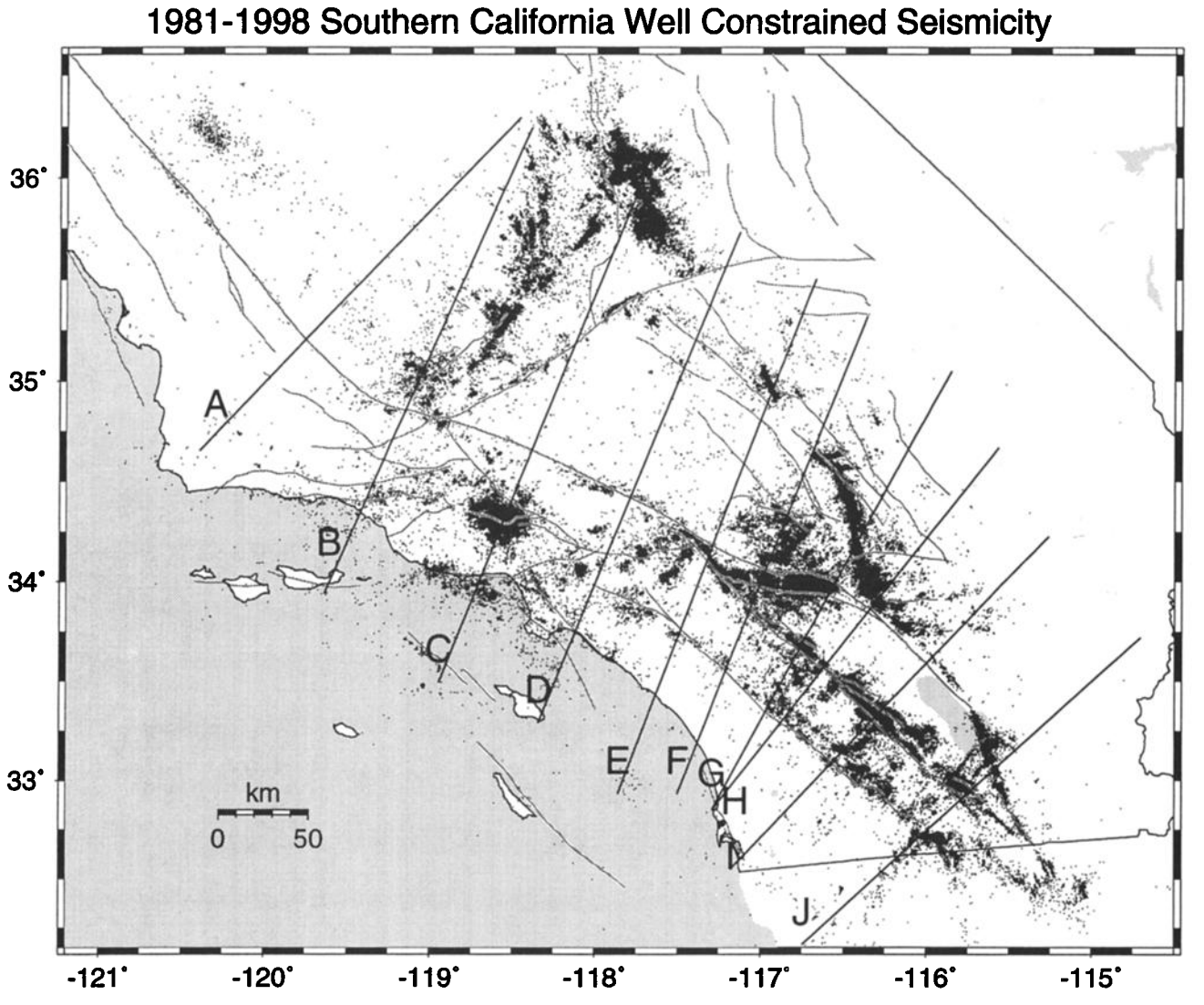

Figure 10. Relocated $M>1.0$ earthquakes from 1981 to 1998. The selection criteria are vertical and horizontal errors ≤3.0 km and minimum distance to the nearest station <4 times the depth, which removes about 39% of the events from the data set of 305,000 earthquakes. Also shown are the locations of depth profiles in Plates 3 and 4. Names of geographical features and faults are shown in Figures 1 and 5.

is most compatible with the Mojave gneiss, suggesting that this lithology is dominant and that schists are only a minor component of the Mojave block.

The V_P profile of the east San Gabriel Mountains is compared to four compositions, Pelona schist, San Gabriel Gneiss, San Gabriel intrusives, and Mendenhall Granulite Gneiss (Figure 11b). The V_P of the east San Gabriels is closest to San Gabriel gneiss and intrusives, suggesting that this lithology dominates the range. The observed V_P profile thus implies that the Pelona schist is only a minor part of the bulk composition of the San Gabriels. Further, the slice at 10 km depth (Plate 1d) does not support fortuitous mixing of Mendenhall Granulite Gneiss with high V_P and Pelona schist with low V_P. In general, our V_P model of the San Gabriel Mountains also agrees with the refraction profile of *Malin et al.* [1981], who found high V_P, consistent with gneiss composition, in the near surface.

Using our 10-km-deep depth slices, we find a complex distribution of V_P and V_P/V_S that is inconsistent with a large underplate of schist beneath southern California. The V_P of 6.2 to 6.3 km/s covers most of southern California except for the western Peninsular Ranges, Imperial Valley, the western Transverse Ranges, and the southern San Joaquin Valley. In general, V_P is too high for schist formations to be the dominant lithology, although the presence of small-scale, <15-km-diameter bodies of schist cannot be excluded. Further, the 10-km depth slice of the V_P/V_S model shows many anomalies of small spatial scale length with values of <1.7. These low V_P/V_S anomalies are more consistent with quartz-rich granitic intrusives of limited spatial extent, rather than an extensive body of schist.

McCaffree Pellerin and Christensen [1998] pointed out that the foliation of Pelona schist can cause a maximum anisotropic change in V_P of 0.8 km/s. Such anisotropy is unlikely to affect the results of this study because the inherent averaging in the rays from the earthquakes to the stations will smooth out the effects of anisotropy. *Cheadle et al.* [1986] inferred from seismic reflection data that within the Mojave terrane the Pelona schist foliation is horizontal. This observation suggests that azimuthal velocity variations are absent within the Mojave terrane. In contrast,

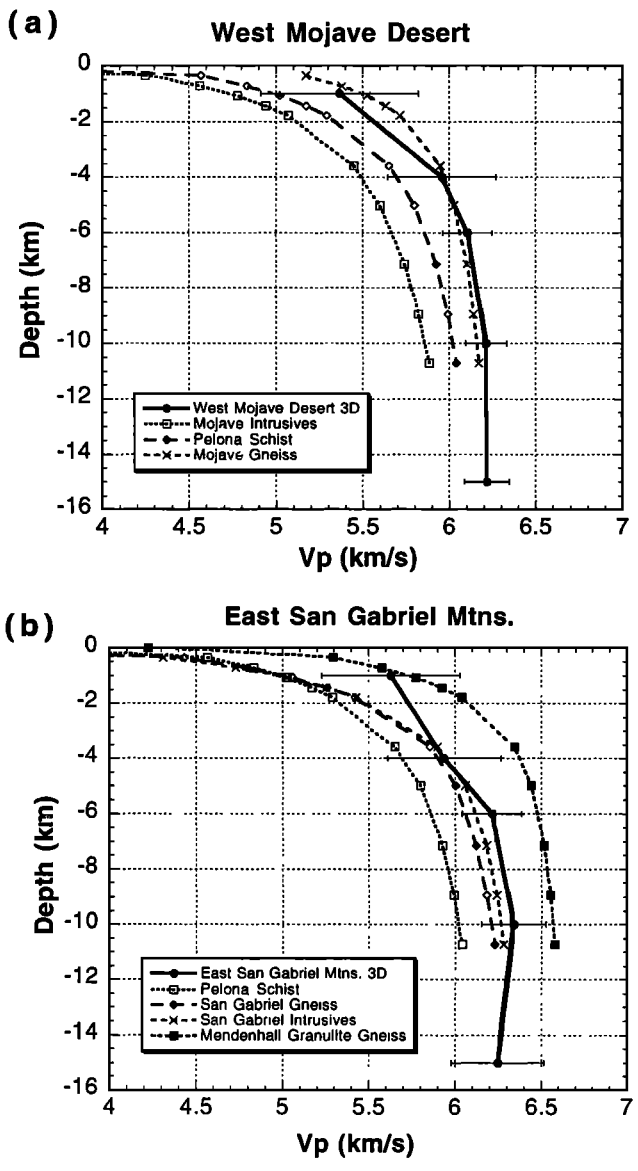

Figure 11. Comparison of V_P depth profiles with double standard deviations shown as error bars for (a) west Mojave Desert and (b) east San Gabriel Mountains with V_P laboratory measurements of V_P in rock samples of known lithology *by McCaffree Pellerin and Christensen* [1998].

Jacobson [1983] showed that the foliation of Pelona schist within the San Gabriels ranges in dip from 45° to 90°. For shallow earthquakes the rays from the hypocenters to the stations are traveling through the schist with subhorizontal ray paths, while rays from deep earthquakes may have steep angles of incidence. Thus, in both the Mojave and San Gabriel terranes the rays from the hypocenters will sample the average velocity of the schist because they have all possible azimuths and a large range of takeoff angles.

The recalculated hypocenters appear to be somewhat shallower to the east of the San Andreas fault or beneath the Mojave Desert (Plate 3). Although *Magistrale and Zhou* [1996] interpreted this as evidence for the presence of schist, we suggest that the depth of seismicity may also be affected by other parameters such as heat flow, strain rates, or regional variations in the ductility of the lower crust.

5.2. Peninsular Ranges Batholith

The 10-km depth layer in the V_P model shows an increase in V_P from east to west across the Peninsular Ranges. To the east, the spatially limited zones of low V_P/V_S and, in general, lower V_P suggest the presence of quartz-rich granitic intrusions. To the west the zones of high V_P of 6.7 to 7.0 km/s suggest the presence of Cretaceous and Jurassic intrusive rocks [*Howell and Vedder*, 1981]. Thus intermixing of rock formations may have occurred along the eastern edge of the Continental Borderland and the western Peninsular Ranges. Such mixing is suggested by *Gastil* [1975], who showed how the metamorphic and plutonic rocks within the Peninsular Ranges batholith form axial symmetric zones with mafic rocks such as gabbroic intrusions more frequent to the west. He suggested that in the western Peninsular Ranges, fusion of both older oceanic crust, as part of subduction, and the associated clastic wedge was contributing to magma generation. In an alternative model, *Hey* [1998] suggested a propagating rift as a mechanism for transferring oceanic lithosphere onto the North America plate. This capture of a subducted slab could have produced shear stresses sufficient to rift the continent and facilitate gabbroic intrusions to the west.

The trend of increasing V_P from east to west also agrees with the findings of *Fuis and Mooney* [1990], who synthesized data for a profile extending across the Continental Borderland and the Peninsular Ranges. To the west they interpreted Franciscan assemblage overlying mafic crust in the Continental Borderland. They hypothesized the west half of the Peninsular Ranges batholithic block to be underlain at depth by mafic (island arc or oceanic) crust and the east half to be underlain at depth by intermediate continental, possibly Precambrian rocks.

To the northwest the high V_P of the Santa Monica Mountains is consistent with paleomagnetic and other geologic data that suggest clockwise rotation of the Santa Monica Mountains block, away from the Peninsular Ranges [*Luyendyk et al.*, 1980]. A similar sharp V_P increase is also present at the San Joaquin Valley-Sierra Nevada transition, corresponding to the western Upper Jurassic arc rocks that are mapped along the western Sierra Foothills belt and are inferred to underlie the southern San Joaquin Valley [*Ruppert et al.*, 1998].

5.3. Eastern Boundary Zone of the Continental Borderland

The most prominent discontinuity in the crustal structure beneath southern California is between the Continental Borderland and onshore California. The crustal thickness changes from an average of 20 to 25 km beneath the Continental Borderland to an average of 28 to 32 km [e.g., *Fuis and Mooney*, 1990; *Richards-Dinger and Shearer*, 1997] approaching the interior. To the northeast below the Sierra Nevada the crustal thickness, however, may increase to 40 km [*Wernicke et al.*, 1996]. The width and location of the transition zone between these crustal provinces are not well constrained. Our V_P and V_P/V_S models provide some constraints on this transition zone because they extend across significant parts of the continental interior and the adjacent Continental Borderland.

The broad distribution of V_P of 6.7 to 7.8 km/s in the 22-km-deep layer along the westernmost Transverse Ranges, Ventura Basin, Santa Monica Mountains, and the Los Angeles basin suggests that the transition zone from the Continental Borderland to the continent is ~30 to 80 km wide in this region (Plates 1e, 1f, and 1g). Farther to the south along the western Peninsular Ranges, the V_P model suggests that the transition zone is narrow, 20 to 30 km wide. The V_P/V_S model is less clear, although in

general terms it shows a broad zone to the north and somewhat narrower zone to the south of elevated V_P/V_S values consistent with the *Vp* model.

Other studies, using seismic reflection profiles or wide-angle data, show a similar progression of width of the transition zone from north to south. *Fuis* [1998], who summarized the results of two crustal reflection and refraction profiles from central and southern California, showed that in central California the increase in crustal thickness occurs over a distance of 20 to 30 km, between the offshore Hosgri fault and the coast line. Beneath the western Transverse Ranges, *Keller and Prothero* [1987] showed that the crust in the Santa Barbara Channel thickens from 23 to 32 km thick over a distance of 50 to 60 km, along a north south profile. Similar thickening of upper and lower crust is observed along the LARSE I line that crossed the Los Angeles basin to the northeast, where the increase in thickness occurs over a distance of 60 to 80 km [*Fuis*, 1998].

The Santa Monica Mountains and the adjacent Ventura and Los Angeles basins are areas where the transition zone is widest and the most complex geological structures exists along the coast line. The Santa Monica Mountains have both anomalous V_P and V_P/V_S structures which is consistent with the volcanic and extensional tectonic history of the range [*Yeats*, 1981; *Crouch and Suppe*, 1993]. Our models agree with the interpretations of *Namson and Davis*, [1988], who showed that the Channel Islands are the westward continuation of the Santa Monica Mountains anticlinorium.

Crowell [1976] proposed that Neogene oceanic crust is present at shallow crustal levels beneath the Santa Barbara Channel and possibly extends beneath the Ventura basin. Our results confirm his interpretations and the findings of *Keller and Prothero* [1987], who found V_P of 7.0 to 7.2 km/s extending up to shallow depths of 20 km and in rare cases beneath the Channel Islands to a depth of 10 km. The 6.0 to 6.9 km/s V_P could be gabbro and other oceanic crystalline rocks while the lower crustal 7.0 to 7.5 km/s material could be oceanic mantle [*Keller and Prothero*, 1987]. The high V_P/V_S anomaly in the eastern Santa Barbara Channel is consistent with the presence of mafic rocks.

6. Discussion

The new V_P and V_P/V_S models presented here show that the velocity structure of southern California is complex. We find that past tectonic processes, such as large lateral offsets along the strike-slip boundary faults, extensional tectonics, and compressional tectonics, account for some of this complexity. To provide further validation for our models, we also compare them to selected models of other parts of California.

6.1. Strike-Slip Tectonics

A series of east to northeast striking cross sections, centered on the San Andreas fault, (SAF) through the V_P and V_P/V_S models show complex velocity structure (Plates 3 and 4). In general, this asymmetry consists of higher V_P to the west of the SAF and more uniform and somewhat lower V_P to the east of the SAF. South of the Transverse Ranges, this transition occurs gradually from east to west, across the San Andreas, San Jacinto, and Elsinore faults. The V_P/V_S is also more heterogeneous to the west of the SAF. Similarly, the depth of the seismicity, with deeper events to the west side of the SAF, also reflects this east-west asymmetry.

The cumulative geological offset along the San Andreas fault of >300 km [*Irwin*, 1990] since the lower Miocene suggests that there should be a significant change in the velocity structure across the fault. Across the SAF, an upward rapid change in regional V_P isosurfaces occurs from the Mojave desert on the east side to the Peninsular and Transverse Ranges on the west side (Plate 5). In particular, the 6.7 km/s V_P isosurface, which could be interpreted as the boundary between the upper and lower crust, rises gradually up from 26 to 15 km depth. The Mojave Desert and a thin north-south corridor along the axis of the Peninsular Ranges are clearly different from most other parts of southern California in that the crust of V_P of <6.7 km/s extends down to depths of at least 28 km. The deepest part of 6.7 km/s isosurface beneath the San Bernardino Mountains may mirror a localized increase in the depth to Moho, presuming that the lower crust is at least a few kilometers thick.

The eastern California shear zone (ECSZ) is a broad region of strike-slip deformation (Figure 1). The trend of low V_P extending across the Mojave Desert from northeast edge of Coachella Valley to Coso is a feature that has been pointed out in previous studies (Figure 1). For instance, *Zhao and Kanamori* [1992] pointed out the apparent correlation between volcanic activity along the east side of the Mojave Desert and lower velocities in their 10- and 22-km-deep layers. The low velocities of the ECSZ thus may form a zone of weakness that concentrates high tectonic strain rates [*Sauber et al.*, 1986].

6.2. Extensional Tectonics

Beneath parts of southern California late Cenozoic spreading events with different timing may have influenced underplating of thinned crust and thus created high-velocity lower crust. Several independent studies, mostly using wide-angle data, have documented high V_P bodies beneath the southern San Joaquin Valley, the Tehachapi Mountains, and the sedimentary basins. Using data from reflection and refraction surveys, *Malin et al.* [1995] suggested magmatic underplating in the Tehachapi Mountains. They argued that crustal uplift and associated erosion affected the region and caused emplacement of lower crust or high velocity bodies at shallow depth. To the north the *Ruppert at al.* [1998] profile also showed a major feature of high V_P beneath the southern San Joaquin Valley. The seismicity extends down to depths of >20 km below the San Joaquin Valley, suggesting that these bodies have a deep brittle-ductile transition zone, consistent with a cooled mafic lower crust.

Similar areas of late Cenozoic crustal extension that existed beneath the major basins of southern California also show signatures of high V_P and, in some cases, high V_P/V_S. For instance, two separate smaller anomalies of high V_P at shallow crustal levels are found beneath the Los Angeles basin and the Ventura basin. These regions may have been unroofed, thinned, and underplated with mafic material in the middle Miocene as a result of block rotations [*Luyendyk et al.*, 1980], or rifting [*Crouch and Suppe*, 1993].

Today, the Imperial Valley region is characterized by extensional tectonics, allowing upwelling of higher-velocity material, as inferred from previous reflection profiles [*Parsons and McCarthy*, 1996]. These zones of high V_P and V_P/V_S are also present in our tomographic model at depths of 15 to 20 km. In contrast to the Los Angeles and Ventura basins, nearly all the seismicity in the Imperial Valley is shallower than 10 km (Plates 3 and 4). The 5- to 6-km-deep basin at the surface and high-

velocity floor beneath the Salton Trough, as mapped by *Parsons and McCarthy* [1996], are also seen in this study. The models presented here are also consistent with a crustal interpretation of the Salton Trough by *Fuis and Mooney* [1990], who inferred, from top to bottom, sedimentary rocks, thermally metamorphosed rocks, and gabbro generated at an onshore spreading center.

6.3. Compressional Tectonics

The most prominent region of compressional tectonics in southern California are the Transverse Ranges. The noticeable lack of coherent signature of the Transverse Ranges from east to west is consistent with the different origins of the terranes that constitute the Ranges. As an example of their complexity *Sorensen* [1985] argued that the southwesternmost Transverse Ranges region, which includes Santa Cruz Island, the Santa Monica Mountains, and the margin of the Los Angeles basin, is underlain by Jurassic igneous and metamorphic rocks such as the 162-m.y.-old mafic Willows Plutonic Complex, 141-m.y.-old metavolcanics of the Santa Cruz Island Schist, and late Oxfordian to early Kimmeridgian metasediments of the Santa Monica Formation. *Sorensen* [1985] inferred that these are fragments of one or more island arc plutonic/volcanic complexes. This complexity is also present in the V_P and V_P/V_S models, particularly beneath the Santa Monica Mountains.

Other parts of the Transverse Ranges are also characterized by heterogeneous velocity structure. There appears to be a sharp transition east of the Ventura basin across the San Gabriel fault. To the west, the velocity structure of the Transverse Ranges is consistent with the adjacent Coast Ranges. To the east, the velocities beneath the San Gabriel Mountains are similar to the transition zone between the western and eastern Peninsular Ranges. These velocities are also similar to what is observed in the eastern Mojave Desert. The V_P profile beneath the San Bernardino Mountains is somewhat lower than elsewhere in the Mojave (Figure 6).

Several major basins are located within or adjacent to the Transverse Ranges. Although the shapes of the basins are only recovered approximately by these models, their location and size are in good agreement with the results of previous studies. The near-surface geology dominates the rapid variations within the 5.5 km/s V_P isosurface (Plate 5). The major basins (Ventura, Los Angeles, and southern San Joaquin) are clearly reflected as depressions within this surface down to depths of 8 km. Mountain ranges are reflected as apparent highs within this isovelocity surface, showing that the V_P of 5.5 km/s reaches the ground surface.

At middle to lower crustal depths the major features of the V_P and V_P/V_S models are the lack of a distinct signature of the crust beneath the Transverse Ranges as opposed to the Peninsular Ranges. The 6.0 km/s V_P isosurface has the least topography, ranging from 2 to 8 km deep, suggesting that it may form the major regional refractor for *Pg* in southern California (Plate 5). The major basins, however, are still apparent as isovelocity lows though less pronounced. The 6.0 km/s V_P isosurface also reflects topographic highs, such as the San Gabriel Mountains, Santa Monica Mountains, Peninsular Ranges, and the southern Sierra. The 6.3 km/s V_P isosurface shows different features as compared with the lower V_P isosurfaces. Only a few areas of high elevation of V_P isosurface of 6.3 km/s extend to depths of 6 km. Most of the V_P isosurface of 6.3 km/s is in the depth range of 6 to 14 km.

6.4. Comparison With Other Parts of California

Several tomographic V_P and V_P/V_S velocity models have been derived for northern and central California by other investigators. These models often employ the same method or are based on more detailed data from seismic refraction and reflection experiments.

Eberhart-Phillips [1990] and *Eberhart-Phillips and Michael* [1993] derived a model for the greater Coalinga and Parkfield areas. These models show similar features as the models presented in this study, with low V_P and high V_P/V_S sediments in the San Joaquin Valley and intermediate V_P values near the San Andreas fault. At depth they also showed high V_P features that possibly represent fragments of the Coast Range ophiolite.

Several recent models derived for the San Francisco Bay area show similar results as we have imaged in the boundary zone between the Continental Borderland and the western Peninsular Ranges. For instance, *Holbrook et al.* [1996] used wide-angle seismic data to show that the Franciscan terranes may be underlain by oceanic crust. In addition, they found a general change in crustal structure across the San Andreas fault, with less complex structure to the east.

The overall complexity of the crustal structure to the west of the San Andreas fault as determined independently by these tomographic models thus appears to extend along most of the length of the California margin, confirming the interpretations by *Fuis* [1998]. Thus the V_P and V_P/V_S tomographic models make it possible to connect the 2-D seismic wide-angle models to provide a 3-D view of the possible range of lithologies and geometrical relationships of major terranes at depth.

7. Conclusions

The 3-D V_P and V_P/V_S models provide new information about the velocity structure at seismogenic depths, ranging from 0 to 25 km, in southern California. The velocity structure is asymmetric with respect to the San Andreas fault. To the east of the San Andreas fault the velocities are lower and show less variations than to the west. Exceptions are the high-velocity crust beneath the southern San Joaquin Valley and extension of the shallow Moho beneath the Imperial Valley to the east and north of the SAF. The San Joaquin Valley may be underlain by old oceanic crust while the Imperial Valley is the site of formation of new crust below a high-velocity lid. The San Andreas fault bounds strong changes in the velocity structure, with lower V_P in the Mojave and western Coast Ranges. The 3-D V_P and V_P/V_S models and the depth distribution of seismicity are inconsistent with an extensive underplate of schist beneath southern California. Within the Peninsular Ranges the velocities increase gradually westward and are highest adjacent to the present coastline. Gabbro or other similar mafic high V_P rocks are present beneath the western Peninsular Ranges. An effect of mixing of Continental Borderland crust with parts of the continent may have created these high V_P bodies at shallow depth. The eastern Peninsular Range appears to be intruded by granitic plutons, as suggested by low V_P/V_S ratios. Although the major basins have low near-surface velocities, they are underlain by high V_P and V_P/V_S, suggesting the presence of mafic lower crust. The near-surface V_P shows significant variations with slow linear increase with depth in the basins and rapid logarithmic increase with depth in areas of hard rock outcrops. Further, the depth to the top of the

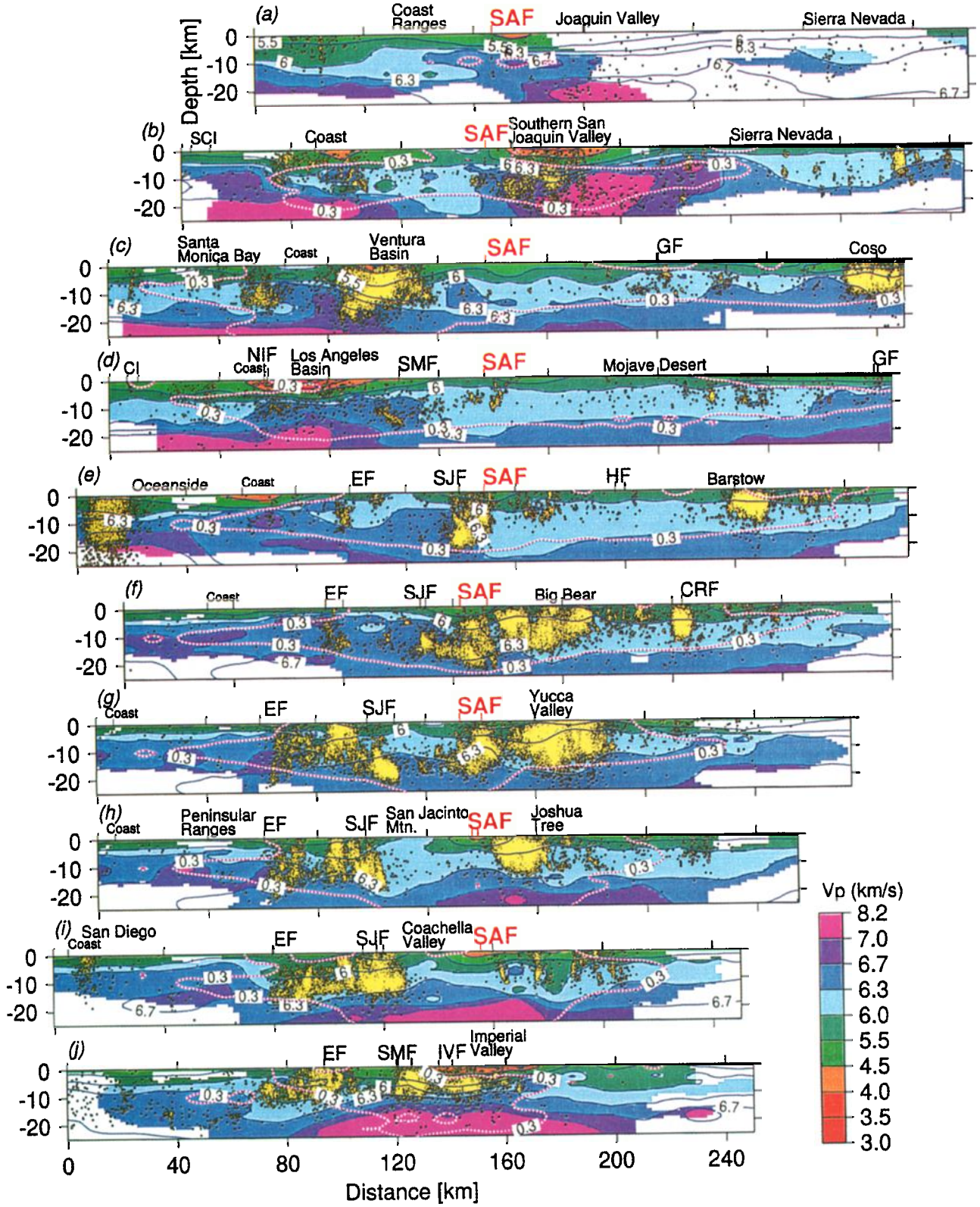

Plate 3. Cross sections through the V_P model aligned along the San Andreas fault, including the seismicity (black circles filled with yellow) within 10 km distance of the profile line. Profile locations are shown in Figure 10. Model areas with adequate ray coverage have DWS values of 1000 or greater and are shown in color; see the appendix. Contour lines of V_P for the whole cross section, including both the well and the poorly resolved parts of the model, are also shown. Heavy short dashed lines are the 0.3 values of the diagonal elements of the resolution matrix, where 1.0 is perfect resolution and 0.0 is no resolution. EF, Elsinore fault; SMF, Sierra Madre fault; IVF, Imperial Valley fault; SAF, San Andreas fault; SJF, San Jacinto fault; CRF, Camp Rock fault; HF, Hellendale fault; NIF, Newport-Inglewood fault; GF, Garlock fault; SCI, Santa Cruz Island. For location of geographical features and faults see Figure 1.

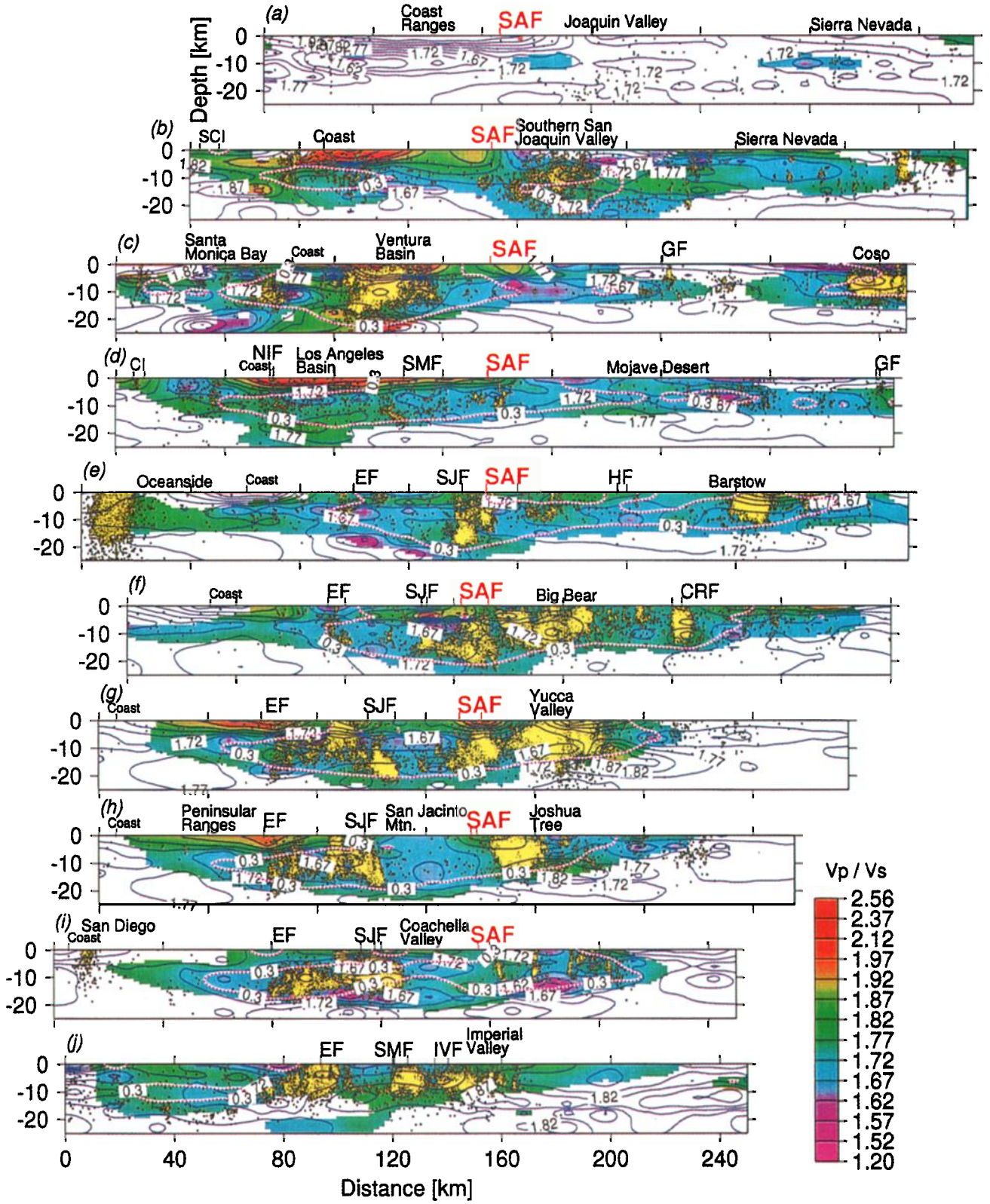

Plate 4. Cross sections through the V_P/V_S model aligned along the San Andreas fault, including seismicity within 10 km distance of the profile line. Model areas with adequate ray coverage have DWS values of 400 or greater and are shown in color; see the appendix. Contour lines of V_P/V_S for the whole cross section, including both the well and the poorly resolved parts of the model, are also shown. Profile locations shown in Figure 10. Heavy short dashed lines are the 0.3 values of the diagonal elements of the resolution matrix. (for abbreviations, see Plate 3).

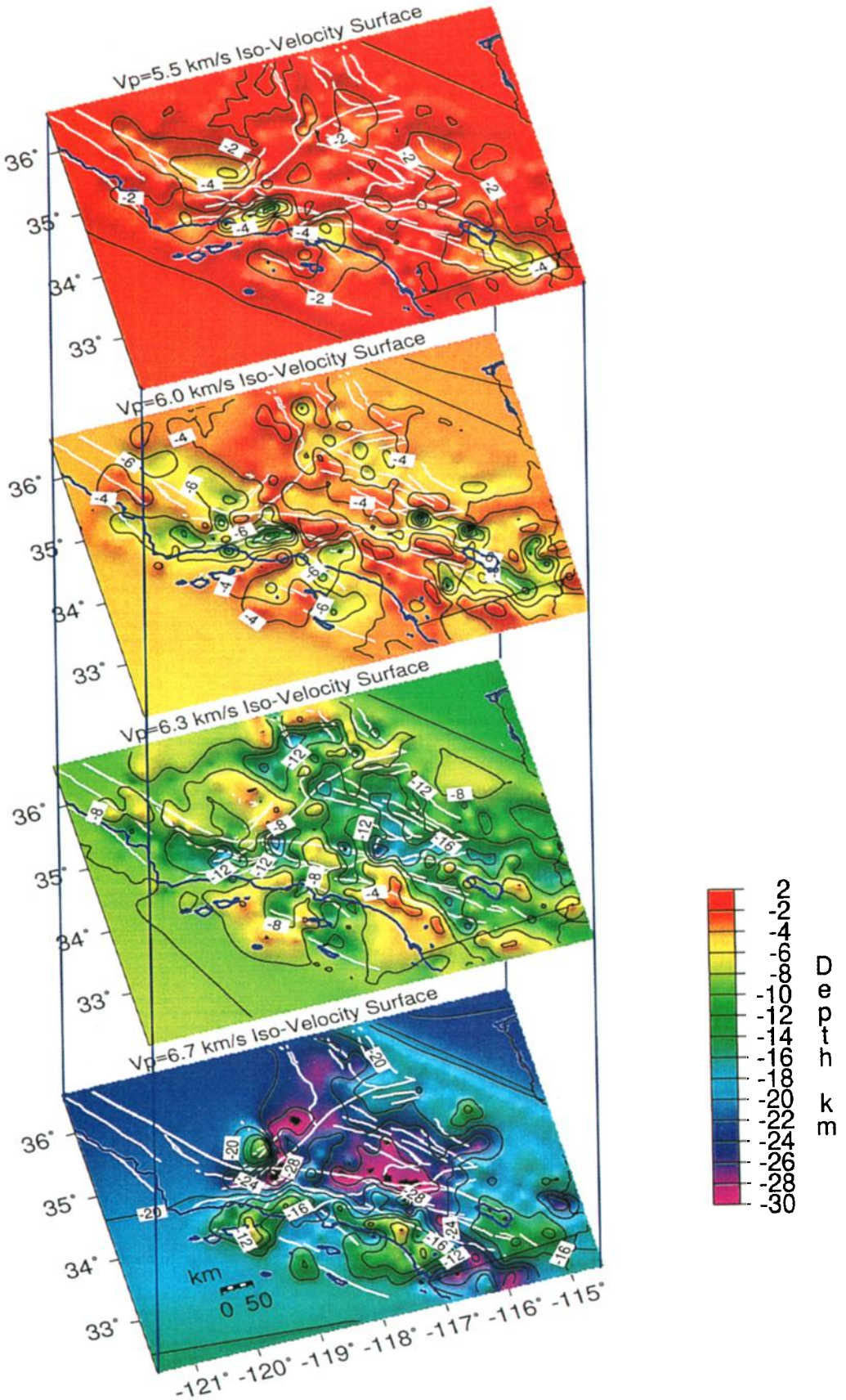

Plate 5. Perspective view of Vp isosurfaces of 5.5, 6.0, 6.3, and 6.7 km/s. The color shading and the black contour lines show the increasing depth of the isosurfaces. Black numbers and contours represent depth below sea level in kilometers. The surface traces (white) of major faults are included for reference. The coast line, state, and national boundary are shown in dark blue.

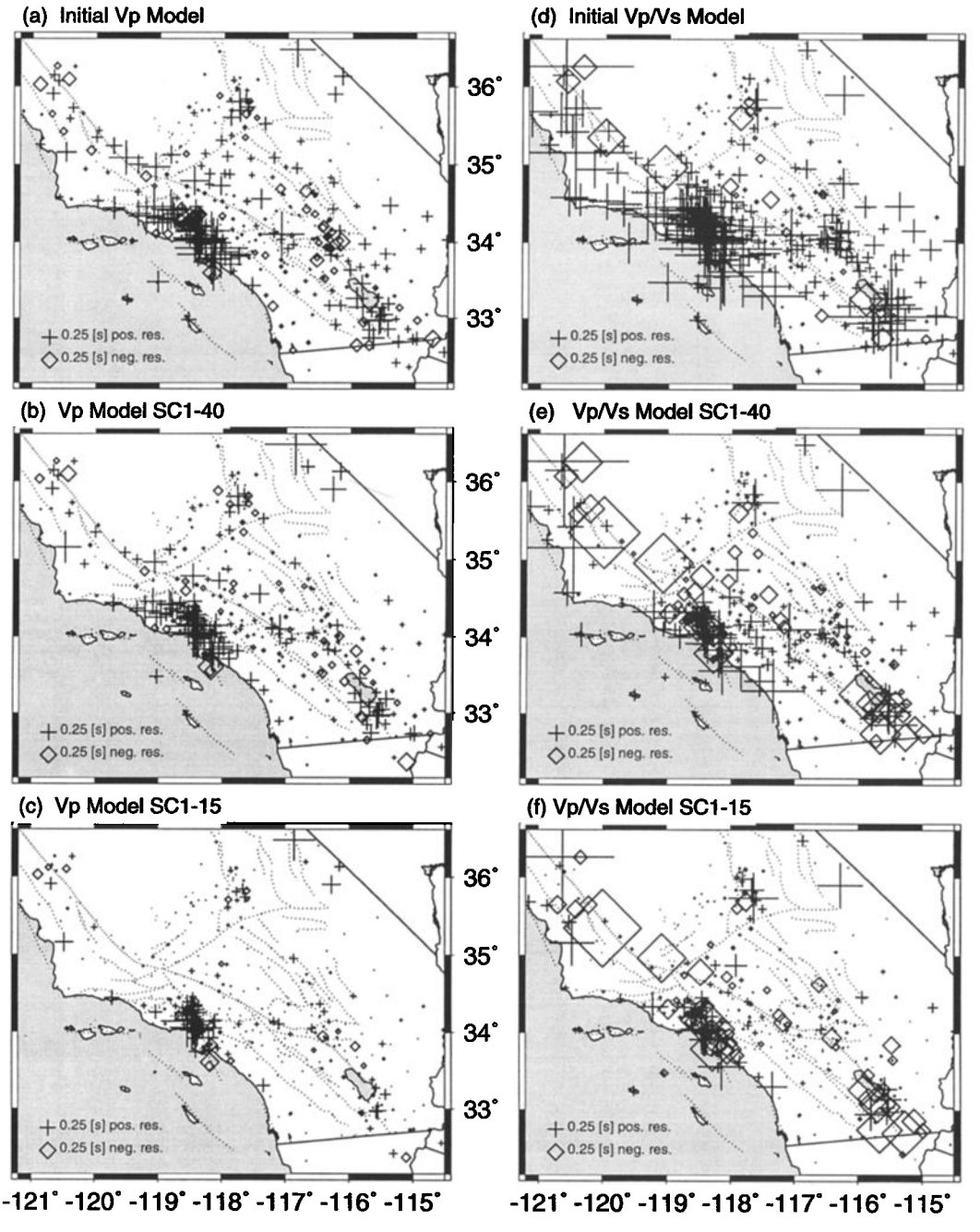

Figure A1. Average station residuals for the *P* and *S-P* arrivals from all events. Major faults shown as short dashed lines. (a) Initial *P* residuals referenced to the 1-D starting model SC0; (b) *P* residuals relative to the 40-km grid 3-D model (SC1-40); (c) *P* residuals relative to the 15-km grid 3-D mode (SC1-15); (d) initial *S-P* residuals referenced to the 1-D starting model SC0; (e) *S-P* residuals relative to the 40-km grid 3-D model (SC1-40); and (f) *S-P* residuals relative to the 15-km grid 3-D model (SC1-15).

lower crust varies across the region showing that changes in crustal thickness involve both the upper and lower crust.

Appendix

A1. Station Delays

The data used in the velocity inversion are the earthquake travel time residuals determined for each event-station pair, which we here refer to as station delays. The inversion reduces these station delays by inverting for a 3-D velocity model with a realistic model length [*Evans et al.*, 1994]. We use the decrease in size of these station delays to demonstrate the quantitative progress of the 3-D inversion. In Figure A1 we show the initial *P* and *S-P* station delays referenced to a flat layered model, the remaining residuals after the inversion for a 40-km grid model and after the inversion for the 15-km grid model.

The residuals show a pattern that corresponds to local geology. The positive *P* delays are observed in basins and other areas with low near-surface velocity. The negative delays indicate mountain ranges and regional anomalies such as the major mountains such

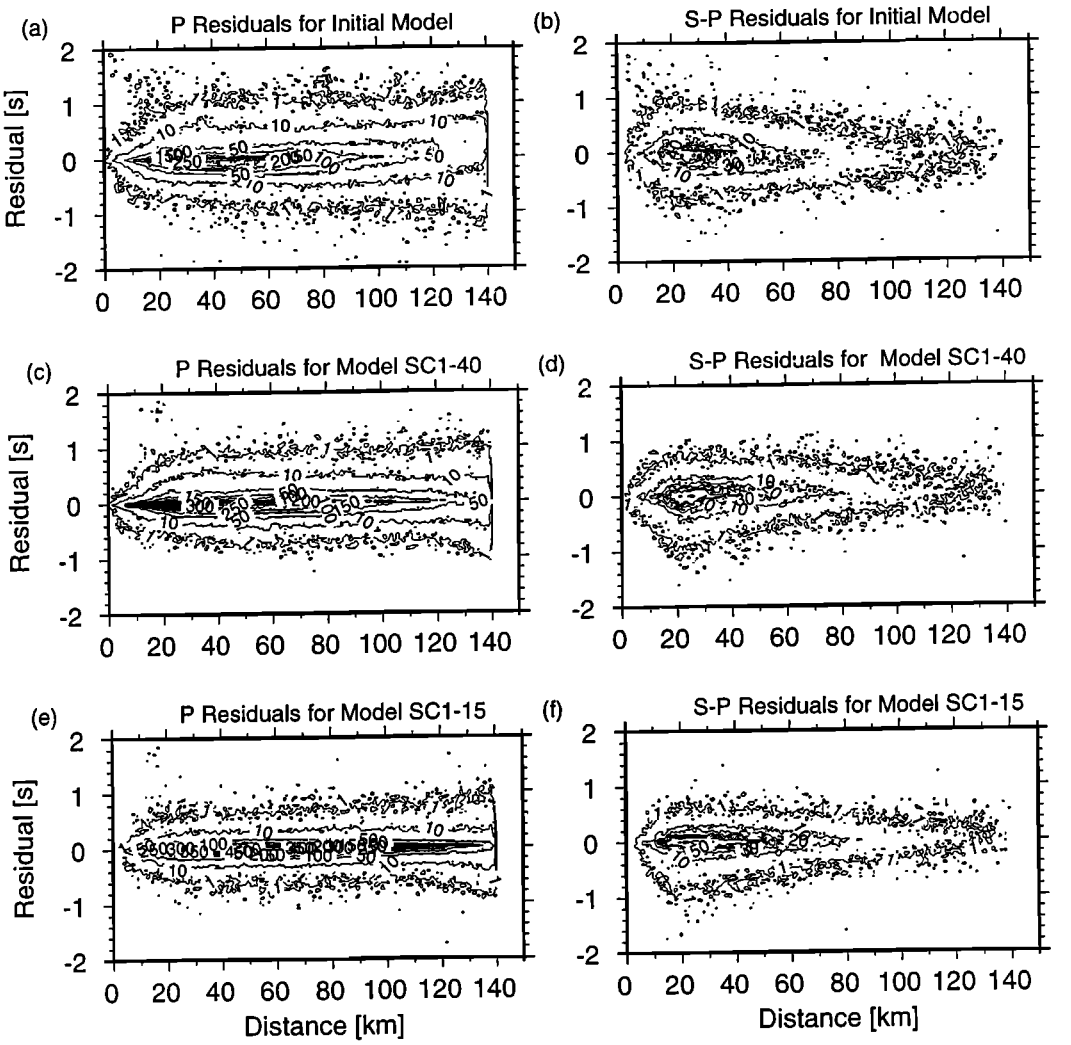

Figure A2. Contour of average station residuals for all the events and all stations used in the inversion, plotted versus epicentral distance for both *P* and *S-P* data sets. (a and b) Residuals referenced to the 1-D starting model (SC0); (c and d) residuals relative to the 40-km grid 3-D model (SC1-40); and (e and f) the residuals relative to the 15-km grid 3-D model (SC1-15).

as the Peninsular Ranges and the San Gabriel Mountains. The *S-P* station delays show similar patterns as *P* delays. The *S-P* delays are larger in value as expected from V_P/V_S, and also in many areas they do not decrease in size. The overall smaller reduction of the *S-P* delays indicates that the error in these data may be large in part because often these *S* arrivals are picked from vertical component seismograms. For instance, converted phases such as *Sp* that precede the true *S*, may be misidentified and picked as *S*.

To identify any systematic biases with distance, we plot the *P* and *S-P* station delays as a function of distance (Figure A2). Visual comparison of the 3-D velocity models with 40-km and 15-km grids shows how these models successively have reduced both the spread of delays and have removed the small bias present in the initial data set.

A2. Inversion Damping

The damping parameter in the inversion keeps a balance between the two factors that the damped-least-squares inversion minimizes [*Eberhart-Phillips*, 1993]:

$$\min(\Sigma r^2 + \varepsilon^2|\Delta m|^2). \quad \text{(A1)}$$

The damping parameter ε is assigned because all the residuals r cannot be transformed into perturbations in the model parameters Δm. With successive iterations, Σr^2 decreases at a different rate than $|\Delta m|^2$ toward zero.

We performed several runs for the 40-km grid to select the most reasonable damping parameter for the inversion [*Thurber*, 1983]. As damping decreases, the resolution increases, and the average standard error increases. We selected V_P damping of 150 and V_P/V_S damping of 15 as a trade-off between the value of the diagonal elements of the resolution matrix and standard errors. The V_P/V_S damping is smaller because the *S-P* data are only 15% of the total data.

During an inversion run the damping value is adjusted after each iteration based both on the initial damping and on current residuals and model perturbations. At the second and subsequent iteration steps we recompute the damping value so that the ratio c

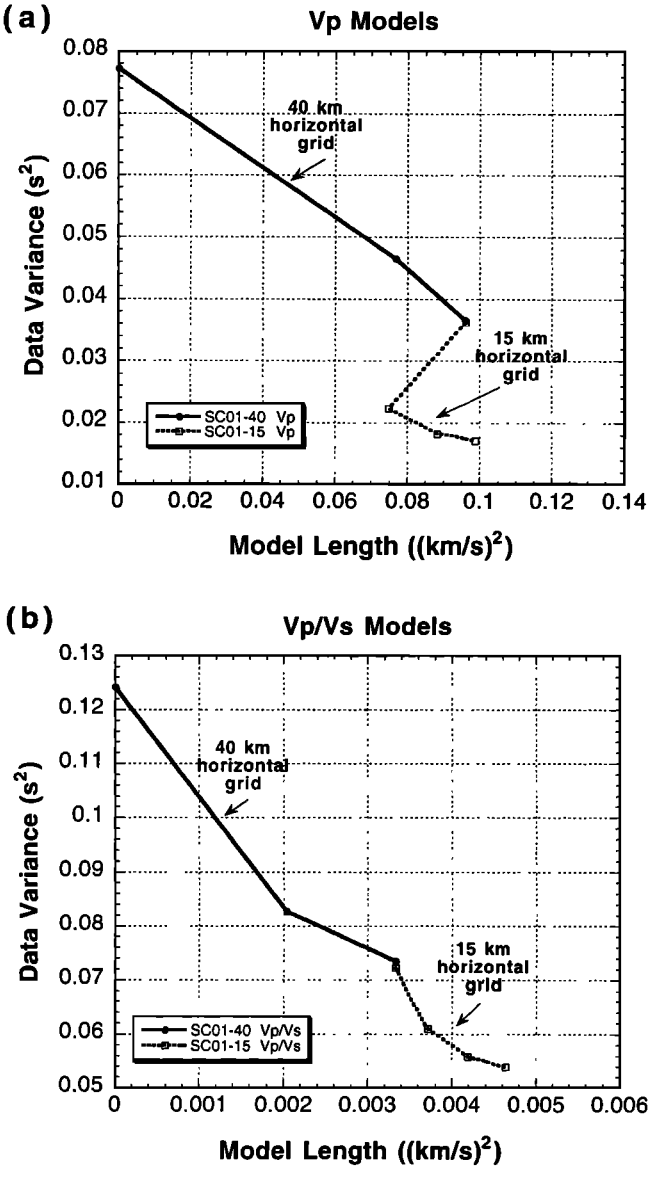

Figure A3. Data variance versus model length for (a) P and (b) S-P data sets for inversions using 40-km and 15-km grid spacing. Values of damping parameter used are also shown.

remains constant [*Eberhart-Phillips*, 1993]:

$$c = \frac{\varepsilon^2 |\Delta m|^2}{\sum r^2}. \tag{A2}$$

These damping values increase with successive iterations because Σr^2 decreases. The data variance decreases as a function of increasing model length with decreasing grid spacing, for a fixed damping value (Figures A3a and A3b). The V_P model length is larger because the V_P/V_S ratio is a smaller absolute quantity with small absolute spatial variations. The two successive 40- and 15-km models reduce the variance, while the overall model length remains approximately the same. The bulk of the increase in the model length is confined to the top layers of the model with smaller variations at greater depths.

Initial test runs showed that if the damping was too high, the model did not change significantly. Conversely, if the damping value is too low, parts of the top two layers of the model would quickly gain unreasonably high velocities at random grid points in the surficial layer of the model. To prevent surficial high V_P zones from forming, which are obvious artifacts within the top layer, the positive velocity perturbations were divided by a factor of 3.0. The effect of additional damping of positive velocity variations within the top layer of the model is to remove artificially high velocities and to reduce the variability within the top layer, making it similar to the variability within the adjacent layers of the model. An alternative method of stabilizing the top layer of the model is to include a layer above the model at the elevation of the topographically highest stations (C. Thurber, communication, 1998).

A3. Evaluation of Model Quality

Factors such as incorrect starting model, parameterization, data errors, ray-tracing methods, uneven ray coverage, and nonlinearity contribute to errors in the final 3-D velocity models and the final 3-D hypocenters. The starting velocity model, parameterization, and nonlinearity were investigated by trying

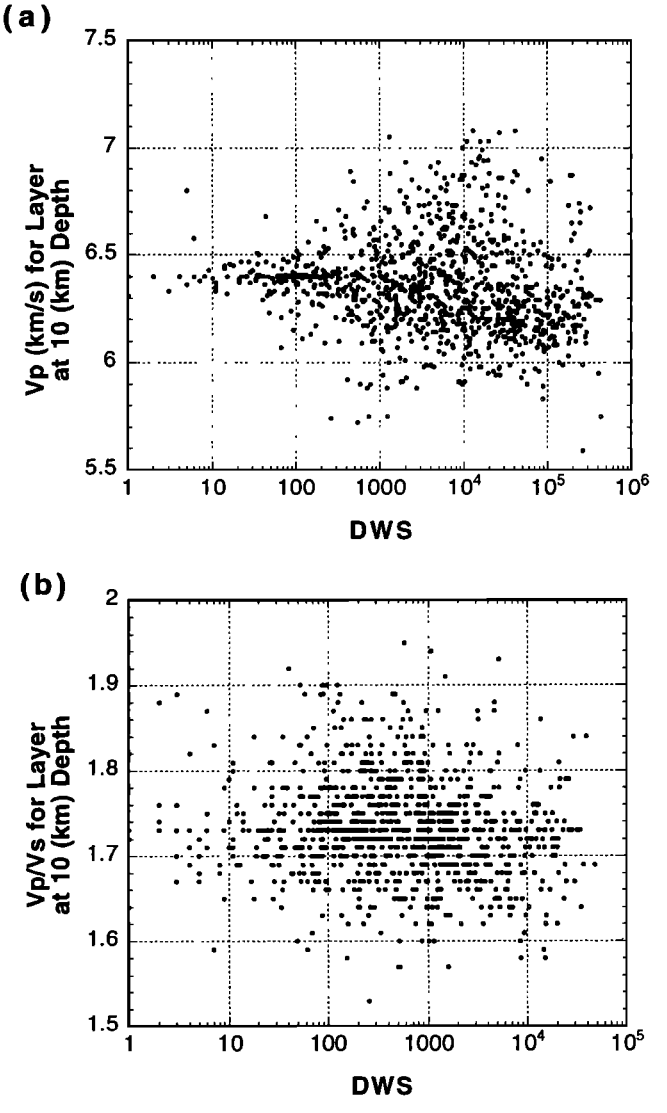

Figure A4. (a) V_P and (b) V_P/V_S values for the 10-km-deep layer of model SC1-15 versus derivative weighted sum (DWS), which is a measure of the ray density next to each node.

different grids, different starting models, and different damping parameters. We have determined the resolution matrix, the derivative weighted sum, and the standard error to evaluate the effects of data errors, ray-tracing approach, and uneven ray coverage.

The model resolution matrix R for our damped-least-squares inversion is [*Menke*, 1989]

$$R = \left(M^T M + L\right)^{-1} M^T M. \tag{A3}$$

where M is a matrix of partial derivatives as described above. If the damping matrix L is zero, the resolution matrix is an identity matrix. The values of the elements of the resolution matrix range from 0 to 1.0, where 0 is completely unresolved and 1.0 is completely resolved. The major parts of the model area of the 15-km grid model has high (0.3 to 0.8). The edges and the southern part of the San Joaquin Valley and the off-shore areas are regions with no station coverage and thus lack significant resolution.

The model standard error provides an estimate of the mapping of the data error into the model error. The model standard error σ is related to the data error σ_d by [*Menke*, 1989]

$$\sigma^2 = (\sigma_d)^2 \mathrm{diag}(C), \tag{A4}$$

where C is the covariance matrix

$$C = (M^T M + L)^{-1}\left[\left(M^T M + L\right)^{-1}\right]^T. \tag{A5}$$

The standard error determined from the covariance matrix varies through the V_P model with errors ranging from 0.01 to 0.03 km/s. When we multiply the standard error by a factor of 2 as suggested by *Thurber* [1983], they range from 0.02 to 0.06 km/s. The V_P variations in the final 3-D model are thus much larger than the standard error of the model. Similarly the V_P/V_S model errors are 0.02 to 0.06 when multiplied by the factor of 2, as discussed above.

We use the derivative weighted sum (DWS) as a measure of the information density provided by the ray coverage. Our values of DWS are larger than reported in other studies because we use many more events than are used in other studies. *Toomey and Foulger* [1989] define the DWS of the nth velocity parameter α_n as

$$DWS(\alpha_n) = N \sum_i \sum_j \left\{ \int_{Pij} \omega_n(x) ds \right\} \tag{A6}$$

where i and j are the indices for the event station, ω is the linear interpolation weight and depends on coordinate position, P_{ij} is the ray path from i to j, and N is a normalization factor for the volume influenced by α_n [*Toomey and Fougler*, 1989].

To explore how the DWS or ray density affects the variations within the model, we plotted V_P for each layer versus DWS at each node. A typical example from 10 km depth is shown in Figure A4. For small values of DWS the V_P and V_P/V_S remain close to the initial value of 6.4 km/s and 1.73. The variations within the V_P model become uniformly large for DWS values of 500 to 1000 and greater. We have chosen to plot the V_P model using color in Plates 1 and 3 for model areas with DWS of 1000 and greater. Similarly, the V_P/V_S model shows uniformly large variations for DWS values of 100. We have chosen a minimum DWS value of 400 to decide where to plot the model. The diagonal elements of the resolution matrix of 0.3 fall within the areas define by DWS 400, and thus the resolution of 0.3 is a more conservative estimate of model quality.

To test the dependence of the final model on the starting model, we used a 5% slower and a 5% faster starting model and determined models. These models did not have significantly higher final data variance than the SC1-40 model.

A4. Spike Test

We used simple layered models with preassigned spikes at one or more grid points to test how well anomalies are reproduced and if artifacts occur such as leaking of anomalies into adjacent nodes. We calculated travel times through models of 40-km horizontal grid spacing that contain one or more spikes of 10% change in V_P or V_P/V_S. In turn, we inverted these synthetic travel times to determine the initial velocity model. In all cases we recovered about 68% to 93% of the amplitude of the V_P spikes when we used damping of 150, and these were located within the well-resolved parts of the model. The V_P/V_S models showed similar behavior with 31% to 65% recovery of the amplitudes with damping of 15. With damping of 1 the recovery of amplitudes was better than 93%, indicating that the amount of leakage between nodes is very small. The spike tests thus show that we can recreate the synthetic anomalies successfully.

Acknowledgments. M. Oskin, J. Hardebeck, L. Jones, and two JGR reviewers, W. Lutter and N. Godfrey, provided comprehensive reviews. This research was supported by U.S. Geological Survey grants 1434-HQ-97-GR-02038 and 99HQGR0039 to Caltech SCEC is funded by NSF Cooperative Agreement EAR-8920136 and USGS Cooperative Agreement 14-08-0001-A0899 and 1434-HQ-97AG01718. Electronic version of the velocity models and the relocated catalog are available from the author or from the Southern California Earthquake Center, Data Center, anonymous FTP at scec.scecdc.org in /pub/hauksson. All maps and cross sections were made using GMT (Generic Mapping Tools) software [*Wessel and Smith*, 1991]. Contribution 8623, Division of Geological and Planetary Sciences, California Institute of Technology, Pasadena. Southern California Earthquake Center contribution 493.

References

Atwater, T., and J. Stock, Pacific-North America plate tectonics of the Neogene southwestern United States: An update, *Int. Geol. Rev. 10*, 375-402, 1998.

Burchfiel, B. C., and G. A. Davis, Triassic and Jurassic tectonic evolution of the Klamath Mountains-Sierra Nevada geologic terrane, in *The Geotectonic Development of California*, edited by W.G. Ernst, pp. 50-70, Prentice-Hall, Englewood Cliffs, N. J., 1981.

Cheadle, M.J., B.L. Czuchra, T. Byrne, C. J. Ando, J.E. Oliver, L.D. Brown, P. E. Malin, and R. A. Phinney, The deep crustal structure of the Mojave Desert, California, from COCORP seismic reflection data, *Tectonics, 5*, 293-320, 1986.

Christensen, N.I., Poisson's ratio and crustal seismology, *J. Geophys. Res., 101*, 3139-3156, 1996.

Crouch, J.K., and J. Suppe, Late Cenozoic tectonic evolution of the Los Angeles basin and inner California borderland: A model for core complex-like crustal extension, *Geol. Soc. Am. Bull., 105*, 1414-1434, 1993.

Crowell, J., Implications of crustal stretching and shortening of coastal Ventura basin, California, in *Aspects of the Geologic History of the California Continental Borderland*, edited by D.G. Howell, *Misc. Publ. 24*, pp. 365-382, Pac. Sec., Am. Assoc. of Pet. Geol, Los Angeles, Calif., 1976.

Eberhart-Phillips, D., Three-dimensional P and S velocity structure in the Coalinga region, California, *J. Geophys. Res., 95*, 15,343-15,363, 1990.

Eberhart-Phillips, D., Local earthquake tomography: Earthquake source

regions, in *Seismic Tomography: Theory and Practice*, edited by H.M. Iyer and K. Hirahara, pp. 613-643, Chapman and Hall, New York, 1993.

Eberhart-Phillips, D., and A. J. Michael, Three-dimensional velocity structure, seismicity, and fault structure in the Parkfield region, central California, *J. Geophys. Res.*, *98*, 15,737-15,758, 1993.

Eberhart-Phillips, D., and J. Mori, The July 1992 seismic calibration experiment along the Landers, California earthquake rupture, U. S. Geol. Surv. Open -file Rep., 94-590, 23 pp., 1994.

Edelman, A., and F. Vernon, The Landers/Big Bear portable instrument aftershock data set, data product report, 52 pp., Univ. of Calif., San Diego, 1992.

Edelman, A., et al., Portable instrument data set from the January 17, 1994 Northridge earthquake aftershock sequence (abstract), *Eos Trans. AGU 75*(44), Fall Meet. Suppl., F457, 1994.

Ehlig, P.L., Origin and tectonic history of the basement terrane of the San Gabriel Mountains, central Transverse Ranges, in *The Geotectonic Development of California*, edited by W.G. Ernst, pp. 253-283, Prentice-Hall, Englewood Cliffs, N. J., 1981.

Evans, J.R., D. Eberhart-Phillips, and C.H. Thurber, User's manual for SIMULPS12 For imaging V_P and V_P/V_S: A derivative of the "Thurber" tomographic inversion SIMUL3 for local earthquakes and explosions, *U.S. Geol. Surv. Open-File Rep., 94-431*, 1994.

Fuis, G.S., West margin of North America—A synthesis of recent seismic transects, *Tectonophysics*, *288*, 265-292, 1998.

Fuis, G.S., and W. D. Mooney, Lithospheric structure and tectonics from seismic-refraction and other data, in *The San Andreas Fault System, California*, edited by R. E. Wallace, *U.S. Geol. Surv. Prof. Pap., 1515*, 206-236, 1990.

Fuis, G.S., et al., Images of crust beneath southern California will aid study of earthquakes and their effects, *Eos Trans. AGU*, *77*, 173, 176, 1996.

Gastil, R.G., Plutonic zones in the Peninsular Ranges of southern California and northern Baja California, *Geology*, *3*, 361-363, 1975.

Given, D. D., and C. L. Koesterer, Station arrival data for a quarry blast on Santa Catalina Island, California, *U. S. Geol. Survey, Open File Rep. 83-462*, 12 pp., 1983.

Hadley, D., and H. Kanamori, Seismic structure of the Transverse Ranges, California, *Geol. Soc. Am. Bull.*, *88*, 1469-1478, 1977.

Hauksson, E., Earthquakes, faulting and stress in the Los Angeles Basin, *J. Geophys. Res.*, *95*, 15,365-15,394, 1990.

Hauksson, E., and J. Haase, Three-dimensional V_P and V_P/V_S velocity models of the Los Angeles basin and central Transverse Ranges, California, *J. Geophys. Res.*, *102* ,5423-5453, 1997.

Haxel, G., and J. Dillon, The Pelona-Orocopia Schist and Vincent-Chocolate Mountain thrust system, southern California, in *Mesozoic Paleogeography of the Western United States*, edited by D. Howell and K. McDougall, pp. 453-469, Pac. Sect. Soc. of Econ. Paleontol. and Mineral., Los Angeles, Calif., 1978.

Hey, R.N., Speculative propagating rift—Subduction zone interactions with possible consequences for continental margin evolution, *Geology*, *26*, 247-250, 1998.

Holbrook, W.S., W. D. Mooney, and N. I. Christensen, The seismic velocity structure of the deep continental crust, in *Continental Lower Crust*, edited by D. M. Fountain, R. Arculus, and R. W. Kay, pp.1-34, Elsevier Sci., New York, 1992.

Holbrook, W.S., T. M. Brocher, U.S. ten Brink, and J. A. Hole, Crustal structure of a transform plate boundary: San Francisco Bay and the central California continental margin, *J. Geophys. Res.*, *101*, 22,311-22,334, 1996.

Howell, D. G., and J. Vedder, Structural Implications of Stratigraphical Discontinuities across the southern California Borderland, in *The Geotectonic Development of California*, edited by W.G. Ernst, pp. 535-558, Prentice-Hall, Englewood Cliffs, N. J., 1981.

Irwin, W. P., Geology and plate-tectonic development, in *The San Andreas Fault System, California*, edited by R. E. Wallace, *U.S. Geol. .Surv. Prof. Pap., 1515,* 1990.

Jacobson, C. E., Structural geology of the Pelona Schist and Vicent thrust, San Gabriel Mountains, California, *Geol. Soc. Am. Bull.*, *94*, 753-767, 1983.

Jennings, P., Fault map of California with volcanoes, thermal springs and thermal wells, 1:750,000 scale, *Geol. Data Map 1*, Calif. Div. of Mines and Geol., Sacramento, 1975.

Jones, L. M., Focal mechanisms and the state of stress on the San Andreas fault in southern California, *J. Geophys. Res.*, *93*, 8869-8891, 1988.

Kanamori, H., and G. Fuis, Variations of *P*-wave velocity before and after the Galway Lake earthquake (M_L=5.2) and the Goat Mountain earthquakes (M_L=4.7,4.7) 1975, in the Mojave Desert, California, *Bull. Seismol. Soc. Am.*, *66*, 2017-2037, 1976.

Kanamori, H., and D. Hadley, Crustal structure and temporal velocity change in southern California, *Pure Appl. Geophys.*, *113*, 257-280, 1975.

Keller, B., and W. Prothero, Western Transverse Ranges crustal structure, *J. Geophys. Res.*, *92*, 7890-7906, 1987.

Lutter, W.J., G. S. Fuis, C. H. Thurber, and J. Murphy, Tomographic images of the upper crust from the Los Angeles basin to the Mojave Desert, California: Results from the Los Angeles Region Seismic Experiment, *J. Geophys. Res.*, *104*, 25,543-25,565, 1999.

Luyendyk, B. P., M. J. Kamerling, and R. Terres, Geometric model for Neogene crustal rotations in southern California, *Geol. Soc. Am. Bull.*, *91*, 211-217, 1980.

Magistrale, H., and H.-W. Zhou, Lithologic control of the depth of earthquakes in southern California, *Science*, *273*, 639-642, 1996.

Magistrale, H., H. Kanamori, and C. Jones, Forward and inverse three-dimensional *P* wave velocity models of the southern California crust, *J. Geophys. Res.*, *97*, 14,115-14,135, 1992.

Malin, P. E., M. H. Gillespie, P. C. Leary, and T. L. Henyey, Crustal structure near Palmdale, California, from borehole-determined ray parameters, *Bull. Seismol. Soc. Am. 71*, 1783-1803, 1981

Malin, P.E., E. D. Goodman, T. L. Henyey, Y. G. Li, D.A. Okaya, and J. B. Saleeby, Significance of seismic reflections beneath a tilted exposure of deep continental crust, Tehachapi Mountains, California, *J. Geophys. Res.*, *100*, 2069-2087, 1995.

McCaffree Pellerin, C. L., and N.I. Christensen, Interpretation of crustal seismic velocities in the San Gabriel-Mojave region, southern California, *Tectonophysics*, *286*, 253-271, 1998.

Menke, W., *Geophysical Data Analysis: Discrete Inverse Theory,* Univ. of Calif., San Diego, 1989.

Namson, J., and T. Davis, Structural transect of the western Transverse Ranges, California: Implications for lithospheric kinematics and seismic risk evaluation, *Geology*, *16*, 675-679, 1988.

Nicholson, C., and D. W. Simpson, Changes in V_P/V_S with depth: Implications for appropriate velocity models, improved earthquake locations, and material properties of the upper crust, *Bull. Seismol. Soc. Amer.*, *75*, 1105-1123, 1985.

Nicholson, C., C. C. Sorlien, T. Atwater, J. C. Crowell, and B. P. Luyendyk, Microplate capture, rotation of the western Transverse Ranges, and initiation of the San Andreas transform as a low-angle fault system, *Geology*, *22*, 491-495, 1994.

Parsons, T., and J. McCarthy, Crustal and upper mantle velocity structure of the Salton Trough, southeast California, *Tectonics*, *15*, 456-471, 1996.

Pavlis, G. L., and J. R. Booker, The mixed discrete-continuous inverse problem: Application to the simultaneous determination of earthquake hypocenters and velocity structure, *J. Geophys. Res.*, *85*, 4801-4810, 1980.

Powell, R. E., Balanced palinspastic reconstruction of pre-Late Cenozoic paleogeology, southern California: Geologic and kinematic constraints on evolution of the San Andreas Fault System, in *The San Andreas Fault System: Displacement, Palinspastic Reconstruction, and Geologic Evolution*, edited by R. E. Powell, R. J I. Weldon, and J. Matti, Geol. Soci. of Am., Boulder, Colo., 1993.

Richards-Dinger, K. B., and P. M. Shearer, Estimating crustal thickness in southern California by stacking *PmP* arrivals, *J. Geophys. Res.*, *102*, 15,211-15,224, 1997.

Ruppert, S., M. M. Fliedner, and G. Zandt, Thin crust and active upper mantle beneath the southern Sierra Nevada in the western United States, *Tectonophysics*, *286*, 237-252, 1998.

Sauber, J., W. Thatcher, and S. C. Solomon, Geodetic measurements of deformation in the central Mojave Desert, California, *J. Geophys. Res.*, *91*, 12,683-12,693, 1986.

Silver, L. T., and E. W. James, Geologic setting and lithologic column of the Cajon Pass deep drillhole, *Geophys. Res. Lett.*, *15*, 941-944, 1988.

Sorensen, S., Petrologic evidence for Jurassic, island-arc-like basement rocks in the southwestern Transverse Ranges and California Continental Borderland, *Geol. Soc. Am. Bull.*, *96*, 997-1005, 1985.

Thurber, C. H., Earthquake locations and three-dimensional crustal structure in the Coyote Lake area, central California, *J. Geophys. Res.*, *88*, 8226-8236, 1983.

Thurber, C. H., Local earthquake tomography: Velocities and V_P/V_S —Theory, in *Seismic Tomography: Theory and Practice*, edited by H. M. Iyer and K. Hirahara, pp. 563-583, Chapman and Hall, New York, 1993.

Toomey, D. R., and G. R. Foulger, Tomographic inversion of local earthquake data from the Hengill-Grensdalur central volcano complex, Iceland, *J. Geophys. Res.*, *94*, 17,497-17,510, 1989.

Um, J., and C. H. Thurber, A fast algorithm for two-point seismic ray tracing, *Bull. Seismol. Soc. Am.*, *77*, 972-986, 1987.

Wernicke, B., R. Clayton, M. Ducea, C. H. Jones, and S. Park, Origin of high mountains in the continents: The southern Sierra Nevada, *Science*, *271*, 190-193, 1996.

Wessel, P., and W. H. F. Smith, Free software helps map and display data, *Eos Trans. AGU*, *72*, 441, 445-446, 1991.

Yeats, R., Quaternary flake tectonics of the California Transverse Ranges, *Geology*, *9*, 16-20, 1981.

Zhao, D., and H. Kanamori, *P*-wave image of the crust and uppermost mantle in southern California, *Geophys. Res. Lett.*, *19*, 2329-2332, 1992.

Zhao, D., H. Kanamori, and E. Humphreys, Simultaneous inversion of local and teleseismic data for the crust and mantle structure of southern California, *Phys. Earth Planet. Inter.*, *93*, 191-214, 1996.

E. Hauksson, Seismological Laboratory, 252-21, Division of Geological and Planetary Sciences, 1200 E. California Blvd., California Institute of Technology, Pasadena, CA 91125.
(hauksson@gps.caltech.edu)

(Received June 15, 1999; revised November 23, 1999;
accepted December 20, 1999.)